2008

The effects of low pressure helium ion bombardment on hydrogenated amorphous silicon

Michael William Beckman
Iowa State University

The effects of low pressure helium ion bombardment on hydrogenated amorphous silicon

by

Michael William Beckman

A thesis submitted to the graduate faculty

in partial fulfillment of the requirements for the degree of

MASTER OF SCIENCE

Major: Electrical Engineering

Program of Study Committee:
Vikram L. Dalal, Major Professor
Gary Tuttle
Mani Mina

Iowa State University

Ames, Iowa

2008

DEDICATION

This thesis is dedicated to my mother Denise and my father Dennis for all of their love, support and constant encouragement.

TABLE OF CONTENTS

LIST OF TABLES

LIST OF FIGURES

ABSTRACT

The benefits of low pressure Plasma Enhanced Chemical Vapor Deposition (PECVD) using helium as the dilutant gas were investigated in a variety of conditions to identify the techniques feasibility as a low band gap material yielding deposition method. Films and photovoltaic devices with intrinsic layers processed at lower pressures with helium dilution are thought to possess improved characteristics with lower hydrogen content and lowered optical band gaps. When films are grown at lower pressures in the presence of helium the optical band gap tends to decrease. Amorphous silicon a-Si:H generally has a band gap around 1.75eV. This work intends to decrease this band gap as far as possible. Films grown under these conditions exhibited reasonable growth rates considering the conditions and yielded very good photo and dark conductivity.

It was expected that dilution with helium at low pressure would decrease hydrogen content by increasing ion bombardment. This was confirmed by FTIR results that indicated hydrogen content of 7-9%. Both films and devices were fabricated that achieved optical band gaps around 1.62-1.65eV. Devices exhibited Urbach energies that were typically lower than 50meV indicating a good quality amorphous structure. High current and fill factor was not achieved due to the possibility of an increase in defect density and high series resistances. The cause of high defect density and series resistance was not determined.

CHAPTER 1. INTRODUCTION

1.1 Background

Due to their positive economic and environmental implications, making photovoltaic cells cheaper and more efficient has been of great interest for the past few decades. This research is concerned with producing competitive efficiencies while using very little raw material by depositing only a thin film. Amorphous silicon (a-Si:H) is able to provide a solution to this problem by exhibiting a superior absorption coefficient. This permits extremely thin films (less than 1 μm thick) to provide substantial power while requiring very little material to fabricate. In addition, thin film solar cells can be stacked in a tandem cell structure so that different materials with different properties can be fabricated together on the same substrate to gather as much light as possible from the AM 1.5 G light spectrum[1].

Thin film photovoltaic cells may be fabricated in a variety of ways including but not limited to Plasma Enhanced Chemical Vapor Deposition (PECVD), but all methods of depositing a-Si:H in some way disassociate the precursor silane or disilane into radicals that form a film on the surface of some substrate. Photovoltaic cells can be grown in a variety of geometries as well. Superstrate geometries use the substrate as a window layer for the light while the alternative substrate down geometry (known as the *substrate* geometry) uses the top contact to permit light absorption[25]. Devices created for this research were all fabricated using the substrate growth geometry shown in Figure 1.1.

In this device geometry, under zero light bias, the device acts similar to a normal diode. However, when an incident photon enters the structure by penetrating the top contact and

p+ layer, there is a possibility that the photon will be converted into an electron hole pair. The holes will then drift toward the p+ region and the electrons will drift toward the n+ region. Under short circuit conditions, this will result in a net current flow from the n+ to p+ region proportional to the number of incident photons for a given area and the efficiency of the photo generation. Under open circuit conditions, a charge buildup will occur in the n+ and p+ regions until the drift of electrons and holes is cancelled out by diffusion current. This will result in a measurable voltage. This voltage is typically denoted as V_{OC}.

An incident photon has several different possibilities of action when entering the structure; (1) the photon may be reflected and not even enter the structure; (2) the photon makes it into the structure but is absorbed in the form of a phonon generating heat; (3) if it is not absorbed as a phonon, it may enter the structure and never get absorbed and even reflect back through the entire structure and not get absorbed on its second trip through; (4) it may be absorbed in the intrinsic layer and result in the generation of an electron hole pair. Maximizing the fourth case and minimizing the other cases makes up the majority of the research that is performed in this field.

It is important to note that in order for an electron hole pair to be generated within the intrinsic layer of the device, an incident photon must have energy greater than the band gap of the semiconductor used for the intrinsic layer. This is the main cause of the third case in the previous paragraph. Even if a photon has sufficient energy there is still a finite possibility that it will not be converted into an electron and hole pair. Therefore the ultimate goal is to grow a material that has a high photoconductivity, meaning it responds well to light by producing carriers for electricity under illumination, and has as the smallest possible band gap. Several different strategies have been developed to help improve absorption at longer wavelengths, such as the incorporation of germanium into the intrinsic layer to form an alloy. Germanium incorporation, however, comes at the expense of open circuit voltage and lower photoconductivity at shorter wavelengths of light. Therefore a way to reduce the band gap of

a-Si:H without significantly compromising other important device properties is of great interest and is the goal of this research.

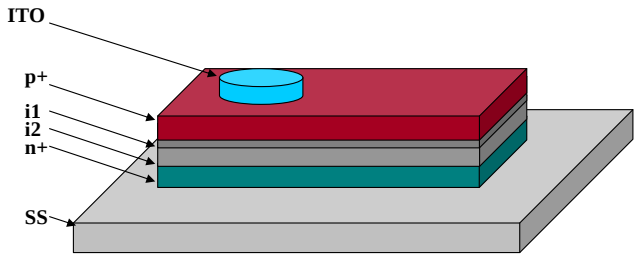

Figure 1.1 Structure of a p-i-n substrate geometry solar cell.

Table 1.1 Device layer descriptions

Layer	Description
ITO	Indium Tin Oxide semitransparent top contact.
p+	Very thin boron doped window layer.
i1	a-SiC:H layer preventing boron and electron diffusion.
i2	Primary photon absorption layer a-Si:H with helium dilution.
n+	Thick phosphorus doped layer encourages EHP drift.
SS	Mechanically polished bottom contact.

1.2 Research Motivation

In order to create devices and films capable of absorbing long wavelength AM 1.5G light, a change to the growth of the intrinsic layer is needed. Specifically, the growth of a low band gap intrinsic layer in a PIN diode arranged photovoltaic device is of great interest. Achieving a lowered band gap in a-Si:H without the use of germanium, while sustaining high fill factors and other device properties is a valuable addition to a tandem solar cell.

One method of growing lower band gap a-Si:H that has not been investigated until now, has been the growth of an intrinsic layer under conditions near the low end of medium vacuum (10-15mTorr) using helium ion bombardment. In essence, it is the deposition of an intrinsic layer via plasma at pressures between 10-15mTorr with helium as a dilutant gas. Several chal-

lenges exist when performing depositions at these pressures, but it is possible that the benefits of a low band gap could outweigh any drawbacks in using this technique.

When using PECVD for deposition of the intrinsic layer (i-layer), 50mTorr and greater is generally used. This is usually performed using hydrogen dilution, where 50mT is sufficient to stabilize a plasma and deposit high quality films. Furthermore, using pressures in the 50mTorr range also increases the deposition rate of the film. Substrate temperatures are generally sustained at about 350°C for the duration of the deposition. These parameters have been shown to create devices and films with excellent results, but with band gaps around 1.75eV.

There are several changes and considerations that must be taken when growing an intrinsic layer under low pressure and using helium dilution instead of using hydrogen at relatively higher pressures. These considerations include the possible instability of the plasma at this pressure. Defect densities may tend to increase due to the increased mean free path of helium ions, resulting in over bombardment. In addition, this unstable or weakly contained plasma may increase the presence of defects by another mechanism. This other cause is due to the ions approaching the ballistic transport regime within the vacuum. When the mean free path of an ion within the plasma becomes greater than the size of the chamber, there is a high probability that some ions may escape the electric field within the plasma. These ions then find a obstacle free path to the walls of the chamber. Upon striking the chamber wall, these ions may release contaminants from the wall of the chamber. These contaminants may then travel into the plasma and be deposited on the substrate and cause defects in the amorphous structure. Therefore it is evident that at lower pressures, the size of the chamber may become an important consideration. To realize devices with very high current and low defect densities, smaller mean free paths for helium ions may be necessary.

Additionally, since the mean free path is larger at lower pressures and more helium ions will be able to bombard the surface, less plasma power should be required to provide sufficient

bombardment. It is also expected that the bombardment of ions on the surface should be much more sensitive to changes in power.

Also, lower pressures result in lower growth rates. While the usage of helium enhances the growth rate at higher pressures, depositing at such low pressures still tends to result in modest growth rates. Since helium is inert, it does not posses the ability to bond with amorphous structure. While this is helpful in that it plays a non invasive role in the resulting film, it may also be a problem due to its inability to satisfy dangling bonds in the amorphous structure. This problem manifests itself with high defect density and overall device quality reduction. This reduction is due to the dangling bonds acting as recombination centers that decrease the diffusion length and carrier lifetime in the intrinsic layer. This is an important consideration due to the objective of this work. However, when depositing at lower speeds, the hydrogen already bonded in the silane gas, may be sufficient for passivation. Furthermore, since hydrogen is a product of the dissociation of silane it can serve as a mechanism to provide passivation of dangling bonds in the film. Another important consideration is that the substrate temperature at low pressure has a different effect than it does at higher pressure. It was observed that the temperature that yields micro-crystallinity in the sample is reduced as pressure is reduced during deposition. Therefore, careful consideration was taken regarding what temperatures could be used. With the necessary deposition parameter modifications in place, working devices were realized at low pressures. These devices possess reasonable growth rates with respect to the pressure being used and exhibit some improvements over higher pressure growth.

1.3 Fabrication with PECVD

PECVD, first introduced by Reinberg, is a modification to conventional CVD with the introduction of a plasma to promote dissociation of precursor gases[2]. CVD has the advantage in that it is capable of depositing very accurately controlled thin films. It is able to accomplish this while still being an economical solution compared to other techniques and

as a result is still widely used in research and industry today. While for the scope of this research, only hydrides of silicon, phosphorus and boron were involved in deposition, PECVD and other flavors of CVD are capable of depositing certain types of metals and ceramics [3]. The main reason for using PECVD is to decrease the temperature required to break down the constituent gases (pyrolysis) and enhance growth rate while still growing a high quality film [3].

While conventional CVD uses thermal activation to initiate the reaction of the precursors, in PECVD the reaction is activated by the presence of a plasma. This is why PECVD is sometimes referred to as Plasma Assisted Chemical Vapor Deposition (PACVD). Since the plasma is assisting in the reaction, the temperature of the substrate can be significantly lower than that of CVD. When growing amorphous silicon, using this lower substrate temperature helps prevent micro-crystallinity. There are different types of plasmas that can be used in PECVD, either arc or glow discharge. Glow discharge is the type that was used in this research, and is favorable because of it's relatively low power requirements when compared to arc discharge and its ability to operated at pressures lower than 2Torr[3]. Glow discharge is considered non-isothermal, that is, the temperature of the system may not remain constant. The plasma is produced using an electrode that has a Radio Frequency (RF) signal applied to it. The signal is in the VHF or Very High Frequency range, and is around 47MHz. This frequency undergoes minor tuning to enhance the stability and output of the power amplifier. Within this plasma, silane, hydrogen and helium, depending on the gases chosen, will become ionized and lose an electron. These loose electrons with temperatures in excess of 20,000K have the ability to produce more free radicals than could have been produced thermally[2]. Since the electron has a relatively low mass, it will be accelerated and oscillate at the frequency of the electric field within which it is contained. These fast moving electrons bombard the precursor gases and break them apart.

This dissociation produces reactive chemicals that can then easily form on the surface of the substrate. Recall that while the substrate is still between 200-400°C, it is relatively cold

when compared to conventional CVD processes and will help prevent unwanted diffusion when using dopants. Also, the ability to work at lower temperatures promotes the growth of amorphous phased silicon, which is of interest for this research. While the incomplete dissociation of precursors in PECVD could be considered a drawback, it can actually serve as an advantage for amorphous silicon by passivating voids in the amorphous structure.

All of the reactant precursors used for the PECVD of a-Si:H are in the hydride group. The interested reader is directed to F. Kampass detailed explanation of ionization induced disassociation[24]. The primary reactant gases are silane, diborane, and phosphine. The formula that describes the reaction that occurs when depositing silicon for the doped layers and intrinsic layer is the following[24]:

Due to incomplete dissociation in PECVD, the following are all possible products of the precursors in order of greatest to least probability:

Silyl Disassociation: $SiH_4(g) \Rightarrow SiH_3(s) + H(g)$

Silylene Disassociation: $SiH_4(g) \Rightarrow SiH_2(s) + H_2(g)$

Silicon Monohydride Disassociation: $2SiH_4(g) \Rightarrow 2SiH(s) + 3H_2(g)$

When depositing n-type layers, the following formula describes the reaction, this is the decomposition of phosphine:

$PH_3(g) \Rightarrow PH_2(s) + H(g)$

$PH_3(g) \Rightarrow PH(s)+H_2(g)$

When depositing p-type layers, the following formula describes the reaction, this is the decomposition of diborane:

$B_2H_6(g) \Rightarrow 2BH_3(s)$

$BH_3(g) \Rightarrow BH_2(s)+H(g)$

$BH_3(g) \Rightarrow BH(s)+H_2(g)$

All of these reactions are considered hydride decompositions[3]. Notice that for all decompositions, there is always a chance of incomplete dissociation. In fact, the probability that the precursor will be completely dissociated is quite small and there is a strong presence of hydrogen bonds even after the reactant chemical has formed at the surface of the substrate. While detrimental in some applications, as stated before, this actually helps passivate any voids in the structure and is the reason that amorphous silicon of this type is considered hydrogenated. From these concepts, there are several deposition parameters that were carefully considered and modified throughout the course of this research. All of these parameters, except for chamber volume can be considered as useable tools for optimizing growth. These are shown in Table 1.2 with their units and description.

Table 1.2 Fabrication parameters

Parameter	**Variable**	**Units**	**Description**
Pressure	P	Torr	Chamber Pressure
Temperature	C	°Celcius	Substrate temperature
Time	t	Minutes	Duration of deposition
Power		Watts	Forward power delivered to the electrode
Flow rate		sccm	standard cm^3 per minute
Relative flow rate		%	Percentage of maximum flow rate
Plasma voltage[1]	V	Volts	Voltage measured from electrode to ground (RMS)
Chamber volume		Liters	PECVD chamber volume (22.74 liters)

1.4 Previous work and literature review

1.4.1 Helium ion bombardment and hydrogen content

Extensive work has been accomplished to model and explain the mass transport mechanisms for PECVD. However, as pressures approach the low mTorr range, typical sequences that describe deposition may no longer apply. This is especially true when using a dilutant gas other than hydrogen. Before investigating these implications, the literary backing behind the rational of using helium and low pressures must be discussed. In Figure 1.2 V. Dalal [4]

[1]Plasma voltage should not be confused with plasma potential.

showed that the usage of helium ion bombardment significantly reduces hydrogen content. This is caused by the helium ions bombarding and breaking the hydrogen bonds from the surface of the amorphous structure[4]. It is therefore expected that if using helium as a dilutant gas, the process of ion bombardment during the deposition should result in a lower hydrogen content. Extensive studies and experiments have shown that a hydrogen content has a positive relationship with optical gap[5-10]. Since a lower band gap is desired, lower hydrogen content is a fundamental goal. In fact work has already been done to model the band gap with respect to hydrogen content by the Penn gap expression[11]:

$$E_{opt} = 1.50 + 1.47C_H \tag{1.1}$$

Since optical gaps below 1.65eV are desired, hydrogen content of C_H less than 10% is desired. This requires effective ion bombardment. The purpose of working at lower pressure can be summed up in the following sentence. Since the chamber pressure has been lowered, the mean free path of heavier helium ions should be sufficient that they are able to more easily reach the substrate and remove surface hydrogen bonds. This is the reason that helium bombardment is being coupled with low chamber pressures.

1.4.2 Ion bombardment-induced damage

The possible implications of low hydrogen content should be a decrease in optical band gap. This however, may come at the expense of dangling bonds in the amorphous structure due to the removal of hydrogen. These dangling bonds act as recombination centers and ultimately hinder current. In addition to helium possibly over bombarding the surface, using the proposed lower pressure can also increase the ion mean free paths within the plasma to levels that may increase ion bombardment-induced damage[12]. This is indicated by an increase in ion density shown in Figure 1.3. It will therefore, be important to verify that the hydrogen content is lower than that of hydrogen diluted a-Si:H but not so low that defect density becomes unreasonably high.

Another plot Figure 1.4 verifies this with an Electron Cyclotron Resonance (ECR) plasma.

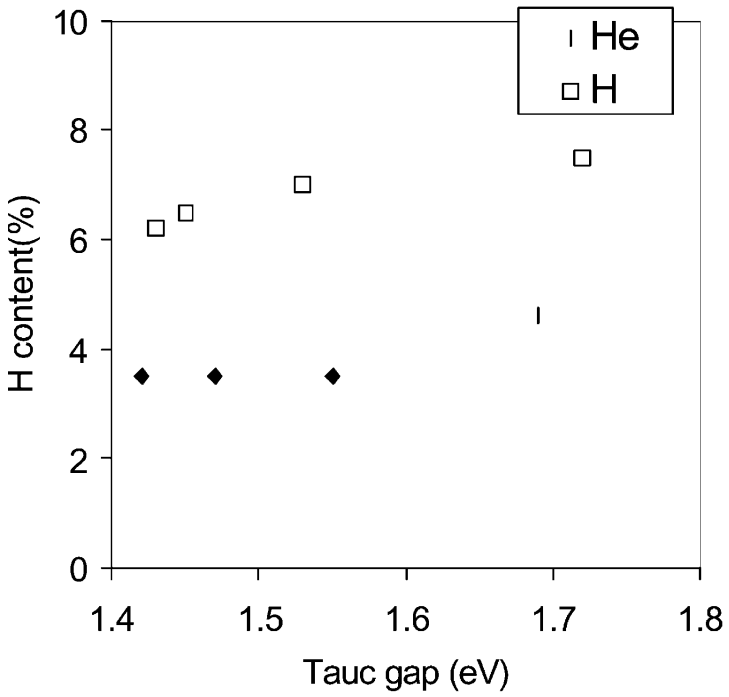

Figure 1.2 Hydrogen content of a-SiGe:H plotted versus Tauc gap with hydrogen and helium as a dilutant gas.[4]

While ECR does fundamentally change deposition parameters, the plasma potential trend can be considered to be similar. According to the plot, working at pressures above 15mT with helium dilution were sufficient to avoid excess ion bombardment-induced damage when using ECR. Ideally the same would hold true for conventional PECVD.

An interesting note is that helium has a relatively high ionization energy compared to that of hydrogen and silane. Helium has an ionization energy of around 24.6eV while hydrogen has 13.6eV[14] and silane has about 12eV[15]. Helium does however have several metastable energy levels that allow ionizations at energies lower than its ionization energy. These energy levels are still quite high in comparison and will pose a problem when attempting to perform helium chemical annealing. It was observed in this work that it was not possible to stabilize a plasma consisting of only helium ions at the working power and pressures for true helium chem-

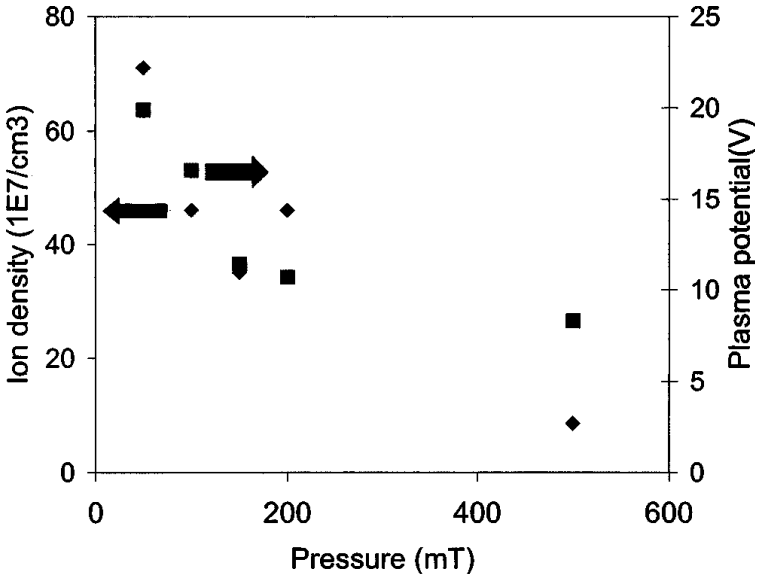

Figure 1.3 Langmuir probe data showing ion density plotted versus chamber pressure. Indicates that both ion density and energy increase with decreasing pressure [12].

ical annealing. To circumvent this problem, a small amount of hydrogen and an increase in power were sufficient to keep the plasma stabilized. However, as a noble gas, helium works well as a dilutant for sustaining a plasma with mixtures of silane, PPM trimethylborate (TMB), and PPM phosphine (PH_3). The main focus of the investigation of previous work is based on the properties of a-Si:H grown using helium and its implications.

1.4.3 Helium dilution effects on growth rate and defect density

Very little work currently exists regarding the use of helium coupled with low pressures. However, it has been explored as being a high growth rate alternative to hydrogen due to its non-etching qualities. Middya et al [13] showed that when using helium as a dilutant gas in the formation of a-SiGe:H films, higher growth rates were observed. Figure 1.5 shows this trend plotted with hydrogen dilution when varying optical band gaps. Middya [13] also indicated that defect densities, when using helium as a dilutant gas, were comparable to defect densities of hydrogen diluted films with the same optical band gaps. It was also observed that the helium

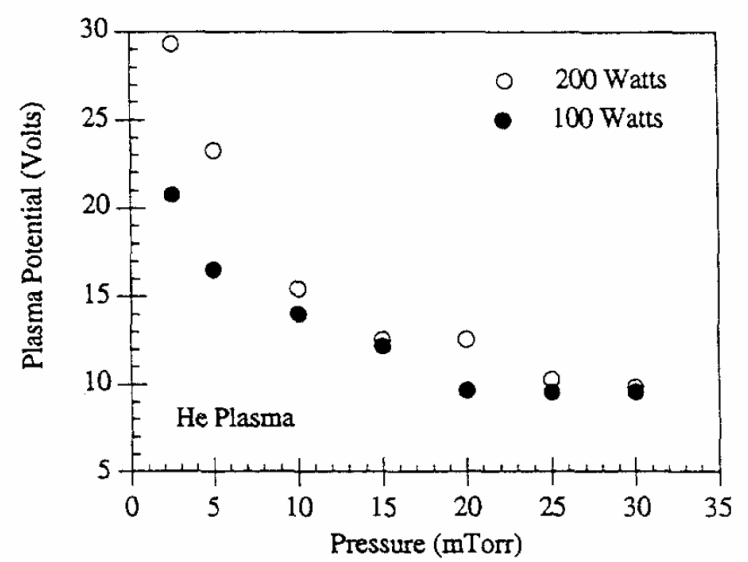

Figure 1.4 Plasma potential versus chamber pressure in a helium diluted plasma [13].

diluted films exhibited improved electron and hole transport properties. This is consistent with the notion that the microstructure of the alloy had improved and that the defects were from different mechanisms.

An obvious question is why helium isnt used as a dilutant gas at higher pressures. This has, in fact, been done and has some applications for those seeking very thick intrinsic layers. Properties at higher pressure with helium dilution, however, do not have the qualities that are considered optimal for highly efficient photovoltaic cells. Pochett et al [16] found that helium as a dilutant gas had a very positive effect on growth rates and reported achieving up to 15 Angstroms per second. A more modest 8 angstroms per second was achieved by using a relatively high pressure ($\approx 550mTorr$), high power ($\approx 15W$) and higher silane flow. With these parameters, Pochett [16] was able to achieve reasonable Urbach energies ($\approx 54meV$) and low defect density ($\approx 9 \times 10^{15} cm^{-3}$) through Photothermal Deflection Spectroscopy. However, this came at the expense of a large E04 gap of about 1.93eV.

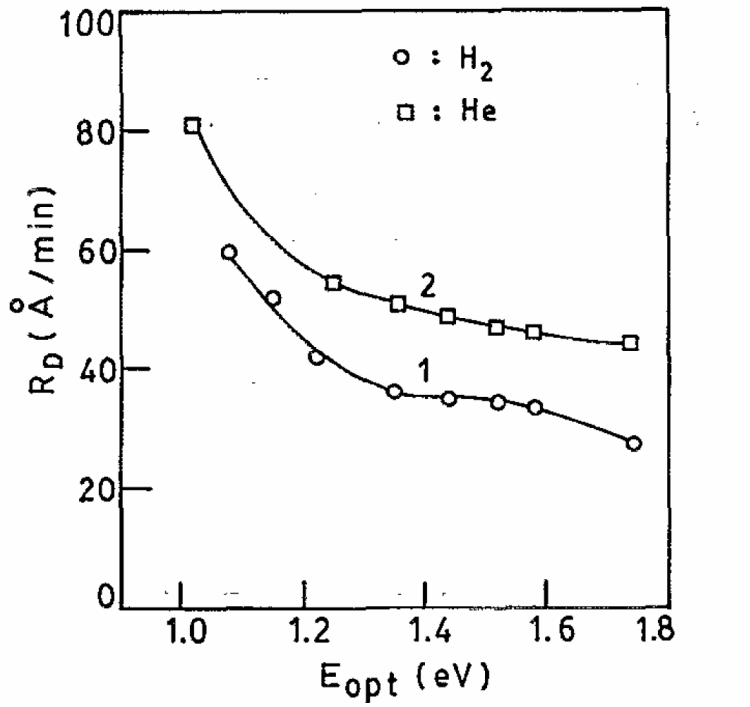

Figure 1.5 High growth rate samples with helium and hydrogen dilution. Plot shows growth rate versus different optical gaps.[13]

This is likely due to large hydrogen content of around 16% along with very low mobilities of around $.3cm^2/Vs$[16]. This indicates a large presence of incomplete silane disassociation in the form of SiH_2 bonds. For Pochetts [16] application of very thick nuclear and x-ray detecting layers, these parameters were not as important. Since the scope of this research is to lower the band gap of amorphous silicon, higher pressures above 50mTorr and high power greater than about $60mW/cm^2$ were avoided. It is likely that decreasing to such low pressures will sacrifice the low density of states in the mid gap realized at higher pressure. This increase in defect density may come from the large mean free path of ions that allows ions to over-bombard the surface.

To that end, Roca et al [17] noted that at low pressures, the effect of increasing power had a smaller effect on growth rate than it did at higher pressures. This indicates that there is no clear advantage in venturing above $60mW/cm^2$ during the deposition. Roca [17] also found

that when using a hot wall reactor that careful control of substrate temperature, while critical, was extremely difficult to control. To compound this problem, Roca [17] also indicated that as the pressure of the chamber increased or decreased with different gases, the temperature of the substrate was significantly affected. For this reason, the effects of different substrate temperatures were avoided due to its unreliability in favor of other parameter effects. It was found that when substrates were maintained between 300°C and 350°C, there was no discernable difference in growth parameters and film quality.

1.4.4 Helium dilution and functional material properties

With a heaver ion, the kinematics of PECVD says that more of the precursor material will be broken down on the surface of the substrate. That is, it is easier for an SiH_2 bond to break with the presence of helium ion bombardment. Kaushal et al [18] showed that using helium with glow discharge produced a-Si:H films with Tauc gaps around 1.67eV as opposed to gaps of 1.75eV seen with hydrogen. Kaushal [18] also stated that reactive ions go deep into a material and perform etching during growth while inert ions like helium remove excess bonded H mainly from the surface. Kaushal [18] also stated that higher substrate temperature for Hot Wire Chemical Vapor Deposition (HWCVD) produced devices with Urbach energies around 46meV. Zhu et al [19] said that in the best a-Si:H films, Urbach energies of 42-43meV were achieved. These positive effects on band gap by removing surface hydrogen may be further improved by chemically annealing to further reduce the optical gap.

1.4.5 Helium chemical annealing

Chemical annealing using hydrogen has been investigated by many research groups as a means of slowing the rate of light induced degradation known as the Staebler-Wronski effect[14]. In the case of hydrogen annealing, an increase in hydrogen content occurs. This will help avoid the Staebler-Wronski effect, but will increase the optical gap, which was shown by Futako et al[5-6]. If inert ions are used during the annealing process instead of hydrogen, the hydrogen content of the material actually decreases. The objective of this research is to try to reduce

the hydrogen incorporation so that the optical gap of a-Si:H can be lowered. Figure 1.6 shows the correlation between hydrogen content and optical band gap[6]. This figure clearly shows the importance of reducing hydrogen content to reduce band gap. Additionally, the usage of a heavy inert ions like argon appears to significantly reduce band gap by ion bombardment. Although these results are for argon, helium should exhibit similar annealing properties by removing excess hydrogen on the surface and decreasing band gap. However, Futako [6] did not comment on all device and film quality measurements. It is possible that films with very low hydrogen content ($\leq$5%) may have undesirable properties. Since using helium as a dilutant gas alone may be enough to lower hydrogen content to around 5%, further chemical annealing may adversely impact parameters by forcing insufficient hydrogen passivation.

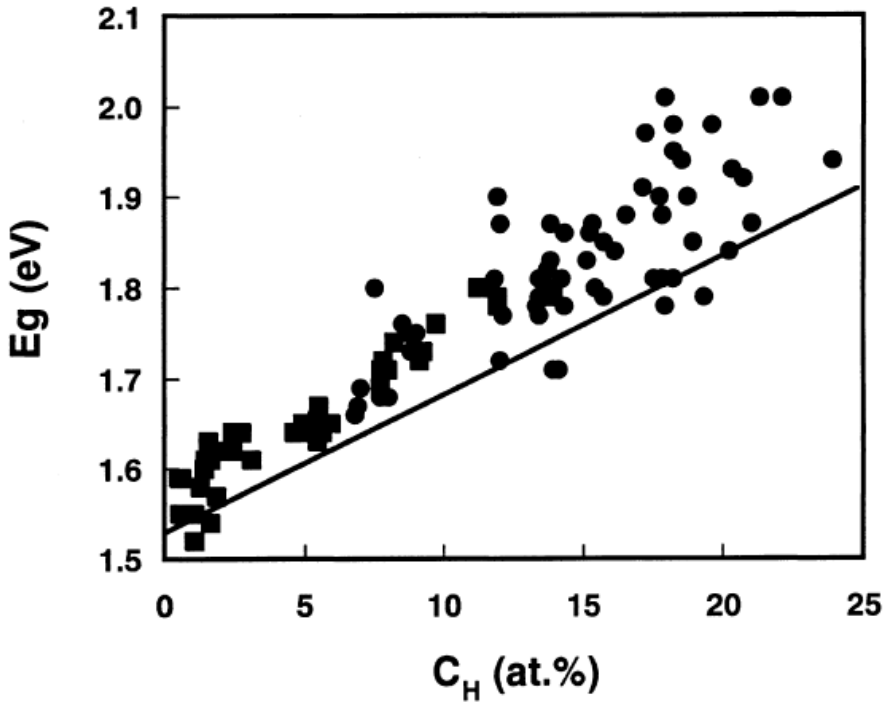

Figure 1.6 Taucs gap versus hydrogen content by atomic percent. Squares indicate annealing with Argon and circles indicate annealing with hydrogen [6].

1.4.6 Other growth parameters that affect optical gap

The first parameter that until now has not been discussed in this work is substrate temperature during growth. Myburg and Swanepoel [20] showed that as substrate temperature is swept from -50°C to 400°C, the incorporation of hydrogen decreases along with Taucs gap. M. K. van Veen et al [23] also found that when depositing at higher temperatures with HWCVD, lower hydrogen content was observed. Therefore, temperatures will be kept above 300°C for the purposes of this research during intrinsic layer depositions. It was also found that as temperature increases, growth rate decreases. Since the effect of increasing temperature has less effect on band gap above 300°C, temperatures for this research will not exceed 400°C [20].

Another parameter that has not been discussed in detail yet is power delivered to the electrode. Myburg and Swanepoel [20] showed that as power increased, optical gap also increased. Therefore it will be important to use a rather modest amount of power during the depositions of the intrinsic layer. Sufficient power will be required to; (1) stabilize a plasma that can disassociate SiH_4; (2) provide enough energy to produce significant helium ion bombardment; (3) provide practical growth rates.

RF also has a strong impact on deposition parameters. Since the frequency of the plasma governs how far a particular ion in a plasma will travel by an inverse relationship, higher power is often required to compensate for very high frequencies. Typically 13.56MHz is chosen as the deposition radio frequency. However for this research 47MHz was used. Therefore it is not possible to directly compare growth rate parameters of systems operating under different radio frequencies. It has been found that around $2.6W$ ($57mW/cm^2$) coupled with 47MHz yields reasonable growth rates and excellent consistency of amorphous phases for the PECVD reactor that was used.

1.4.7 Industry Achievements

Many different research groups both academic and commercial are working in parallel to strive for the best combination of techniques to produce the most efficient solar cell devices. This section is concerned with the investigation of several government and commercial research groups and their achievements.

The National Renewable Energy Laboratory (NREL) has several groups working on the tandem triple junction photovoltaic cell. The group working specifically on a-Si:H has been working to improve device stability, improve efficiency, improve narrow band material quality, and increase deposition rates. The work related to improving narrow material quality is of interest because of its relation to this work. NREL [27] has reported that using a-SiGe:H, Tauc band gaps of less than 1.5eV have been achieved. NREL has also achieved high values well above .9V and fill factors above 60% even after degrading[27]. However the measured current density is a more modest value[27]. This was performed using Hot Wire Chemical Vapor Deposition (HWCVD)[27]. It was found that decreasing filament temperature improved the quality of low band gap devices[27].

Another very well known research group known as Uni-Solar® is also working on improving the quality of a-Si:H devices. Uni-Solar® has reported obtaining Tauc gaps using germanium alloyed a-SiGe:H of around 1.4eV[28]. Uni-Solar® has also reported outdoor efficiencies consistently greater than 6% while ranging temperature from 0-35°C[29]. This proves the viability of this technology in a wide range of earthly climates.

CHAPTER 2. METHODOLOGY AND PROCEDURES

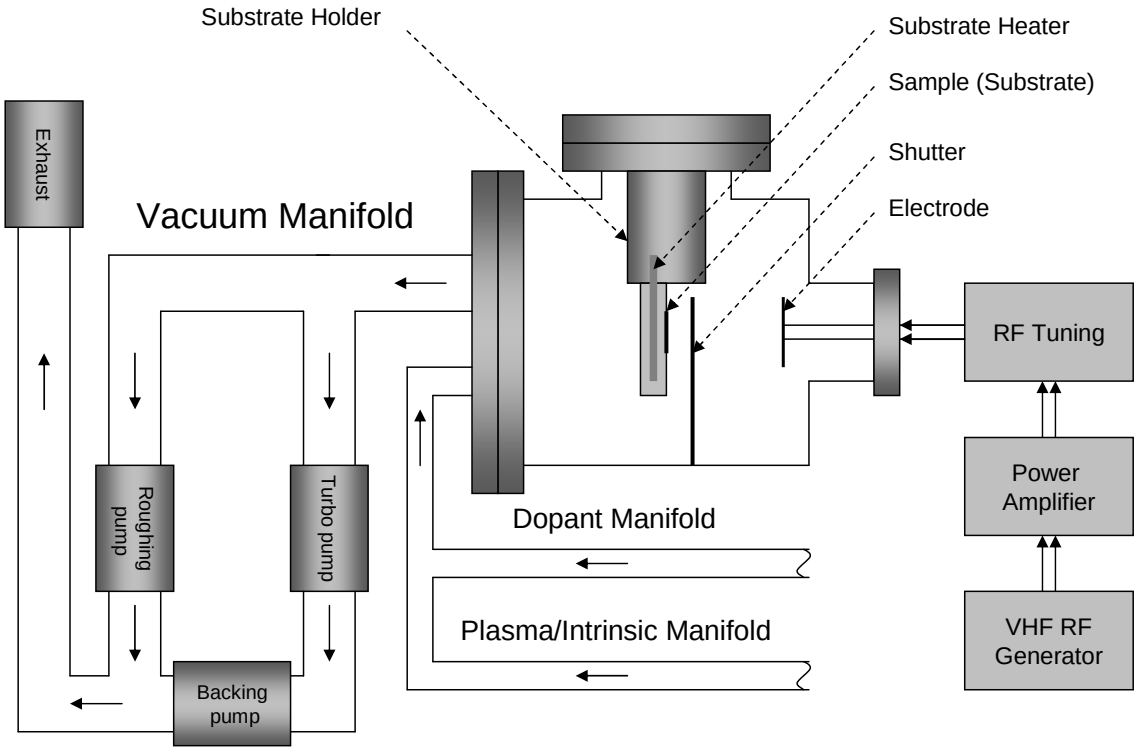

Figure 2.1 PECVD reactor schematic

2.1 PECVD reactor design

The PECVD reactor used for fabrication of films and devices was a glow discharge cold-walled reactor shown in Figure 2.1. This reactor has a horizontal orientation. That is, the electrode that induces the plasma is parallel to the surface of the substrate that is being deposited on and is at a 90 degree angle to the ground. The vacuum and gas flow to the chamber is orientated behind the substrate holder and is also horizontal. This orientation has an advantage in that gravity doesn't encourage foreign objects into the vacuum pump lines, protecting

the rotary and turbo pump assemblies. Also, since the electrode and shutter assemblies are not above the sample, debris is less likely to fall onto the substrate or electrode during a deposition. Because of this orientation, the reactor has a top loading substrate holder. This holder contains the heating elements within it.

An ideal situation would be to keep the reactor at high vacuum all the time and introduce a sample through a series of pressure interlocks. However, such an elaborate system is not necessary if proper purging techniques are used. Without an interlock system, the deposition chamber can at times be exposed to atmospheric pressure. This occurs when the reactor is having a sample loaded, unloaded, or when the reactor is being cleaned. Once loaded, the most economical and practical way to reach a medium vacuum level of around 1 Torr is to use a rotary vane pump. Often known as a roughing pump due to the region of pressure operation that it works in, this pump can quickly bring the chamber from atmospheric pressure to medium vacuum levels. This pump connects to the side of the chamber behind the substrate holder. Since depositions are in the medium vacuum range, but are near the high vacuum range, utilization of a turbo-molecular pump provides the ability to quickly purge and achieve the proper level of vacuum to sustain the desired plasma within the chamber.

The precision when throttling the turbo-molecular pump is quite consistent at pressures less than 1 Torr and above 1 mTorr and can stay at a given pressure for hours with negligible pressure deviation. Given the nature of this research, the ability to hold a consistent vacuum is imperative in obtaining reliable data. The turbo-molecular pump used on the reactor is also a horizontally mounted pump. Behind the turbo-molecular pump is another rotary vane pump that acts as a backing pump. This pump removes gases that have been pulled through the turbo-molecular pump. It also acts as a barrier between the atmospheric pressure exhaust and the high vacuum region that the turbo-molecular pump operates within.

In order to safely operate and monitor the pumps, a set of gauges are employed for accu-

rately measuring pressure. The first gauge is a pressure transducer that operates in regions greater than 1mT. At pressures in the high vacuum range, an Ion gauge is used. The ion gauge has a useful range well below what is required for the reactor. The ion gauge is only used briefly for recording pressures after purges and when the chamber has been thoroughly evacuated. The pressure transducer gauge is useful within the range of pressures used during depositions.

In addition to the elaborate gas removal system, another equally important system is responsible for gas admission into the chamber. A series of gas cylinders store hydrogen, helium, silane, methane, TMB and phosphine. An initial flow regulator brings the pressure from 1000psi and higher to a much lower level depending on the gas. From here, solid metal tubing brings the gas into a more advanced set of flow regulators. These regulators control the amount of gas that is permitted to reach the reactor chamber when gases are enabled.

Given their different uses, there are three different classifications of gas types that enter the reactor. These are intrinsic line gases, plasma line gases, and dopant line gases. Dopants can be parasitic to intrinsic films and are kept separate from the intrinsic and plasma lines until just before entering the reactor. Since the plasma line only carries hydrogen and helium, the intrinsic line merges with the plasma line shortly after gases leave the set of individual flow regulators. Next to the flow regulator control panel is another panel with a series of switches which enables the flow of any of the gases required. There are other gas lines that also enter. One is a N_2 line used to bring the reactor to atmospheric pressure and for purging. In addition to the N_2 line is an O_2/N_2 mixture line that is used to create an oxygen plasma, which has the purpose of neutralizing boron in the reactor.

With a proper gas flow system and vacuum system, some method of producing a plasma is required. This is done by applying 3-7 Watts of RF signal to a 3 inch diameter (76.2mm) electrode that sits opposite the substrate and holder. This electrode is attached to the reactor

wall, but is electrically isolated. A coaxial cable connects to the outside of the reactor and runs from a power meter to a power amplifier. The power amplifier is driven by a signal generator. The reactor is equipped with a shutter that can be moved so that it rests between the substrate and the electrode. This allows plasmas to be ignited without depositing on samples. The substrate holder which contains the heating core also contains two separate thermocouples. The heater automatically adjusts to hold a consistent temperature.

CHAPTER 3. CHARACTERIZATION

3.1 Film Characterization

3.1.1 UV/Vis/NIR spectroscopy

UV/Vis/NIR spectroscopy can measure the absorption, transmission, and reflection of films. This information yields accurate information about film thickness and optical gap. Measurements were performed using the Perkin-Elmer Lamba 9 spectrophotometer. To evaluate a film thickness a plot of the transmitted light as a percentage was plotted over the spectrum of visible to infrared light. This produced a plot with the appearance of an oscillation. The position of the peaks and valleys of the transmittance are characteristic of the thickness of the film (Figure 3.1). The thickness can be evaluated using the following expression:

$$t = \frac{\lambda_1 \lambda_2}{2(\lambda_1 n_2 - \lambda_2 n_1)} \tag{3.1}$$

Where λ_1 and λ_2 are the locations of adjacent peaks in transmission and where n_1 and n_2 are the refractive indexes for the corresponding wavelength of light. The values for n_1 and n_2 are referenced from a table depending on which wavelengths are identified as peaks, and what the approximate band gap of the material is.

Transmission and absorption measurements are not possible with devices, thickness is measured using reflection instead of transmission. In order to minimize the variations in reflection from light scattering from different directions, an integrating sphere is used to provide uniform scattering and effectively remove the effect of light incident from different angles.

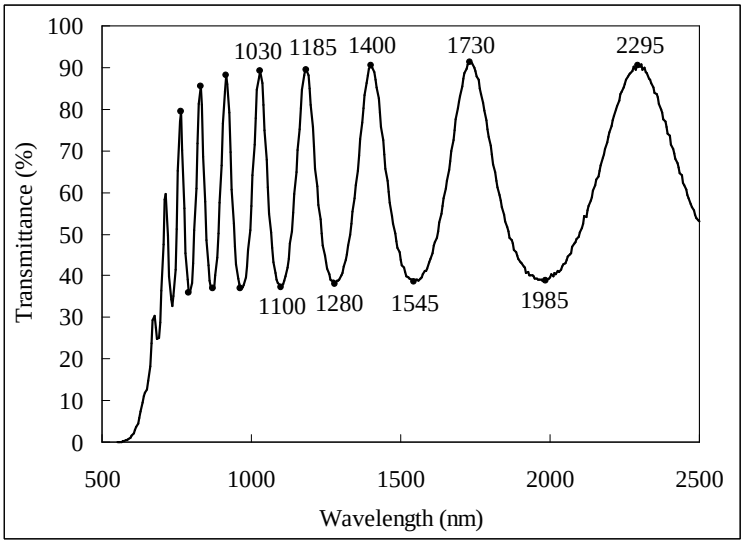

Figure 3.1 Film transmission curve.

The spectrophotometer is actually only able to measure reflection and transmission. Absorption is calculated using the following equation:

$$A(\lambda) = \log_{10}\left[\frac{1}{T(\lambda)}\right] = \frac{\ln\left(1/T(\lambda)\right)}{\ln 10} \tag{3.2}$$

It is also known that transmission is approximately given by the following expression:

$$T(\lambda) = \left(1 - R(\lambda)\right)\exp\left(-\alpha(\lambda)t\right) \tag{3.3}$$

Where $T(\lambda)$ and $R(\lambda)$ are the transmission and reflection respectively measured by the spectrophotometer. The variable $\alpha(\lambda)$ represents the absorption coefficient of the sample and t is the thickness of the film measured by equation 3.1. The absorption coefficient can be solved for as a function of absorption, reflection and thickness from the equations 3.2 and 3.3. This is given by:

$$\alpha(\lambda) = \frac{\ln(10)A(\lambda) + \ln\left(1 - R(\lambda)\right)}{t} \tag{3.4}$$

When plotted with respect to photon energy, absorption coefficient yields the plot in figure

3.2. Unfortunately since no sample is infinitely thick, some oscillation will be observed. By carefully approximating the running average between the peaks, a linear region will appear in the plot. Where this linear region intersects $\alpha = 10,000$ is the measurement known as E04 gap. Since no linear extrapolation is required, the measurement has much lower error, but is actually quite far from the actual optical gap ($\approx$ .15eV). E04 gap serves as more of a reference point for consistency between samples by removing error from the subjectivity of the linear region in the absorption curve. Therefore when expressing trends between devices or films with respect to optical gap, E04 is the preferred due to its high level of precision.

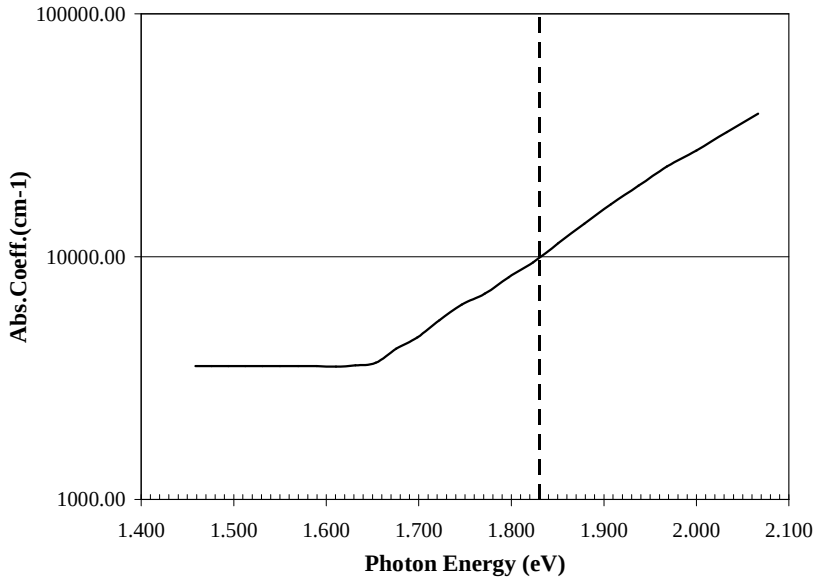

Figure 3.2 E04 gap extraction from absorption coefficient versus. This film possesses an E04 gap of about 1.83eV.

Another more accurate, but also more subjective measurement is that of Taucs gap. Taucs gap is revealed by plotting $\sqrt{\alpha E}$. This yields the plot shown in figure 3.3. When the linear region is extrapolated to the x-axis, the materials optical gap is revealed. This optical gap is known as Taucs gap. Since Taucs gap is closer to the actual band gap of the material, when reporting band gap of individual samples, Taucs gap is the default parameter to report.

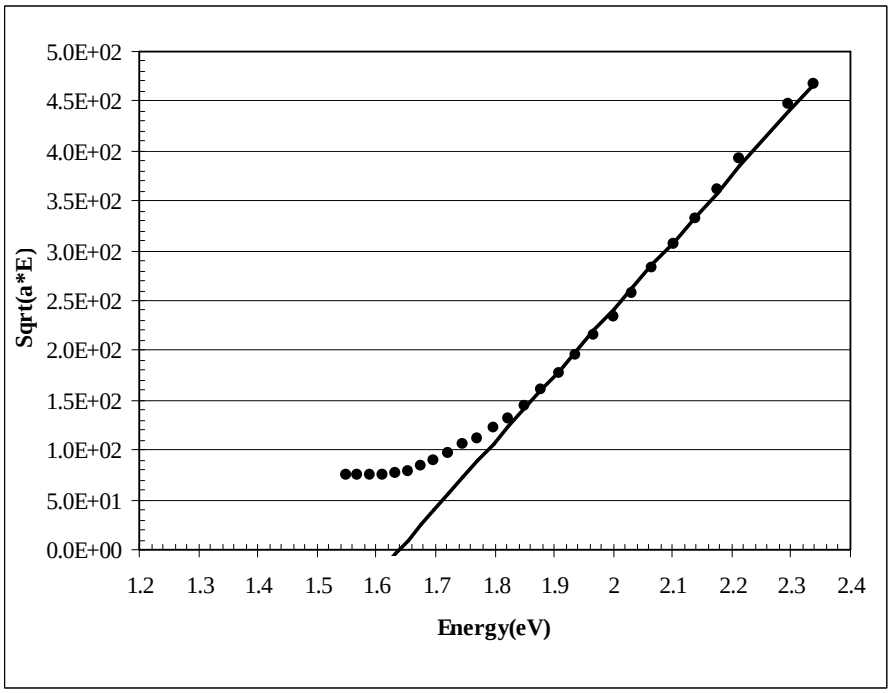

Figure 3.3 Extrapolated linear region for measurement of Taucs gap. This film possesses a Taucs gap of about 1.64eV.

3.1.2 Activation energy

Activation energy was measured by measuring currents given an applied voltage of about 100V at different temperatures. This should not to be confused with activation energy of constituents in deposition. Evaluating activation energy requires initially heating the sample to about 200°C and keeping it there for about 30 minutes. The sample is then allowed to cool. At every 10 degree interval the current is recorded. These different current readings form a straight line when the natural log operation is applied and the slope of that line is characteristic of the activation energy of the material.

$$E_A = E_C - E_F \tag{3.5}$$

$$E_A = \left| \frac{\ln(I_2) - \ln(I_1)}{[1/T_1] - [1/T_2]} \right| k \tag{3.6}$$

The plot of the natural log of current versus inverse temperature yields a linear plot that can be used to evaluate activation energy. This measurement is an indicator of the location of

the Fermi level in the material and is useful in determining whether a material is doped or undoped. Ideally with a band gap of about 1.6eV, the activation energy should be around .8eV, indicating that a material is nearly intrinsic.

3.1.3 Photo/Dark conductivity

To measure the responsiveness to light, measuring the conductivity of a sample under light and dark conditions is useful. This is done by exposing the sample to AM 1.5 G light and recording the current under a 100V bias. A good sample should have 10-100uA of photocurrent given the contact geometries patterned by the chrome evaporator masks. The light is then turned off and the current settles. After a time period of 15-30 minutes, the sample should settle on a value. This is its dark current. A good sample should have dark current in the 10-100pA range. An electrometer is used to supply the voltage bias and to measure the current through the sample. The ratio of these two yields a number that is indicative of the samples relative response to light. Generally a ratio greater than 10E+5 is considered good.

3.1.4 Urbach energy

Since amorphous silicon does not have a well defined single band gap, as indicated in the previous section, it is necessary to identify how clear a band gap is. One way to do this is to evaluate how quickly absorption decreases as the energy of photons is decreased to the band gaps energy. In a perfect crystalline semiconductor, the density of states should fall very sharply, however in an amorphous or nanocrystalline material, the band tails. To gather information about the band tails, a light source is conditioned through a monochromator and a light chopper. This monochromatic chopped light is then focused on the sample. At the same time the sample is under a DC light bias. This DC light bias serves to ensure that photogenerated carriers fill the mid-gap states. This can be observed in Figure 3.4. Since the lock-in amplifier will only measure voltages that are the same frequency as some reference, in this case the chopper, only the voltage increase from the monochromatic light is measured. This not only makes sure that the DC light bias is not counted as photocurrent, but it also removes

any other noise sources including the 60Hz light sources in the background. As the wavelength of light is stepped through longer values, the current output of the cell should decrease. This effect can be seen in Figure 3.5.

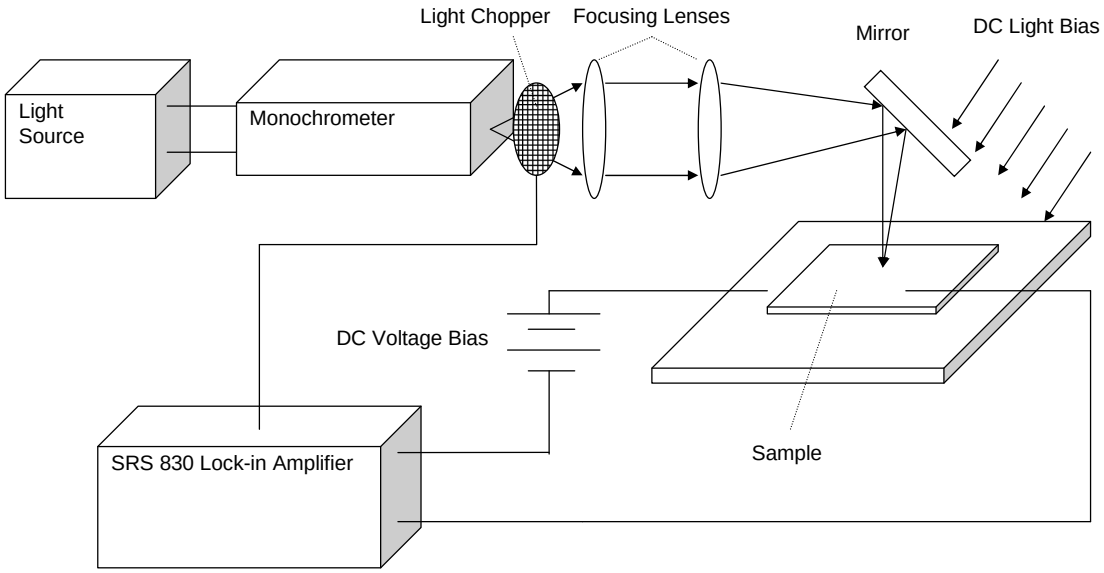

Figure 3.4 Quantum Efficiency measurement setup.

When plotted, a linear region (actually exponential) will appear through the center of the oscillations (see figure 3.5). Urbach energy can then be approximated using the following expression:

$$E_U = \frac{E_2 - E_1}{\ln(10)(\log_{10}(\alpha_2) - \log_{10}(\alpha_1))} \tag{3.7}$$

Where E_1 and E_2 are two different photon energies in the linearly extrapolated line and where α_1 and α_2 are two corresponding absorption coefficients. Generally E_1 and E_2 are chosen so that they lie on decade intervals of α to simplify the calculation. This yields a number generally between 40meV and 60meV. Lower E_U indicates higher material quality. Urbach energy also serves as an indicator of mid gap trap states. These trap levels reveal themselves as a shoulder around 1.3eV. Generally as defect density increases, this shoulder increases in size.

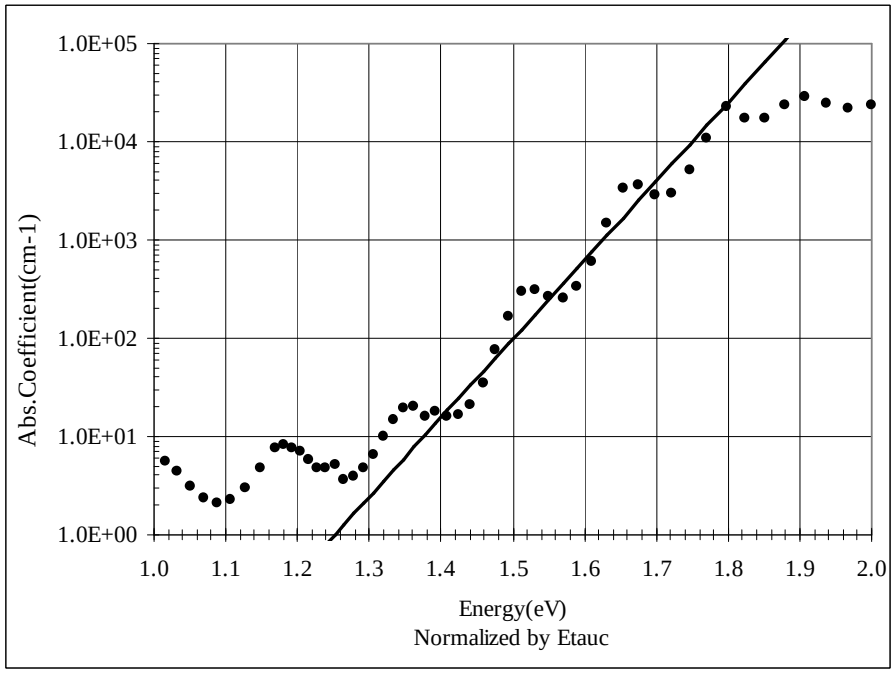

Figure 3.5 Subgap QE plot showing absorption coefficient versus photon energy. Plotted on a log scale.

3.1.5 Fourier Transform Infrared Spectroscopy

Fourier Transform Infrared Spectroscopy (FTIR) is different from Raman scattering in that it actually measures the bonds that are present in a material instead of what chemicals are present. This measurement setup uses an infrared laser to facilitate a resonation within the bonding structure of a material. Similar to resonating a tuning fork by subjecting it to sound equal to its fundamental frequency, the bond resonations yield a time delay. When varying the distance of a reference beam to a mirror, temporal coherence between the reference beam and the beam can be measured. This coherence pattern can then be plotted with respect to wavenumber. This yields the plot shown Figure 3.6. All peaks are characteristic of some type of set of bonds. This is especially important when determining hydrogen content because it yields information about the relative ratio between SiH_2 bonds and SiH bonds. Therefore from the plot below, the ratio of peak 5 to peak 6 indicates the SiH:SiH_2 ratio. Good quality films have large SiH:SiH_2 ratios (≥ 4).

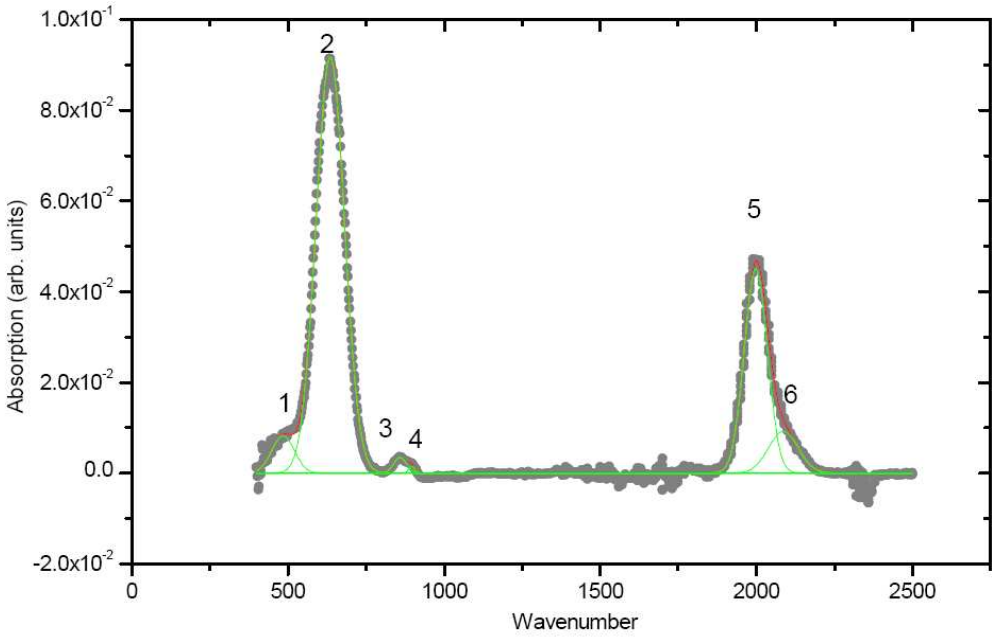

Figure 3.6 IR spectra for helium diluted a-Si:H film grown at 350°C.

Work performed by Brodskey et al [30] related hydrogen content by atomic percentage of a-Si:H to the resulting IR spectra. Brodskey indicated that the integration of peak 2 of the IR spectra, which is centered on 640/cm yields the total hydrogen content of the film. This integration follows the following expression.

$$N_H = A \int \frac{\alpha(\omega)}{\omega} d\omega \tag{3.8}$$

Where α is the absorption coefficient, ω is the wavenumber, and A is an experimental constant. The resulting number is a percentage. It should be considered that a large amount of subjectivity is realized throughout the hydrogen content calculation. Not only is it difficult to accurately evaluate the thickness, the accuracy is also affected by how well the peak fitting routine actually resembles the hydrogen peak. Brodskey also indicated that the relative magnitudes of the 2000/cm and 2085/cm peaks corresponded to the relative content of SiH and SiH_2 bonds respectively. When the ratio of the 2000/cm and 2085/cm peak is taken, it yields the ratio of SiH to SiH_2 bonds where SiH bonds are desired[30].

3.2 Device characterization

3.2.1 Devices I-V curves

One of the first measurements that is often used to determine gross failures and overall functionality in a photovoltaic cell is the current versus voltage measurement or IV measurement. This measurement yields information about the devices fill factor (FF), short circuit current (I_{SC}), and open circuit voltage (V_{OC}). I_{SC} measures the current that flows when both sides of the PN junction are at the same potential. As voltage is increased in forward bias eventually the current will fall to zero. This point is considered V_{OC}. FF is a measure of how well the actual device follows an idea diode curve which is governed by equation 3.9 where V_m and I_m are the corresponding voltage and current where power delivered is maximum. Total efficiency can be calculated from equation 3.10 where P_{IN} refers to power incident on the surface of the photovoltaic cell.

$$FF = \frac{V_m I_m}{V_{OC} I_{SC}} \tag{3.9}$$

$$\eta = \frac{I_{SC} V_{OC} FF}{P_{IN}} \tag{3.10}$$

IV measurements also yield information about the series resistance of the solar cell, as well as the shunt resistance. Series resistance can be approximated by evaluating the slope of the linear region near V_{OC}. Shunt resistance is calculated from the slope of the linear region at negative voltages. Shunt resistance is characteristic of collection in the i-layer and should be as flat as possible.

3.2.2 Quantum efficiency and subgap quantum efficiency

Quantum Efficiency or QE along with its sub gap counterpart are likely the greatest contributors to information about device performance and material structural properties. Qualitatively, QE is the ratio of collected carriers at a particular wavelength to the number of incident photons. This is generally expressed as relative QE where the entire QE measurement is normalize to the peak absorption keeping all values less than 1. This removes a large amount

of variation between samples and makes comparison more straight forward. QE measurements use the same physical system as the sub gap measurements shown in Figure 3.4. However the method of data manipulation is different. The expression in equation 3.11 shows the relationship between QE, absorption α, film thickness t, $\mu\tau_{eff}$ product, and the electric field across the depletion region $E(y)$.

$$QE(\lambda) = \int_0^t \alpha(\lambda) \exp(-\alpha(\lambda)x) \exp\left(-\int_0^x \frac{1}{\mu\tau E(y)} dy\right) dx \tag{3.11}$$

The QE measurement is conducted over the entire usable range of the device. Since under normal operation a solar cell will be biased near its max power point, another .5V biased QE measurement is taken to see how well absorption occurs when the electric field is reduced. Ideally the biased absorption should be equal to the unbiased absorption. However in practice ratios of 0V bias over .5V bias less than 1.2 are acceptable.

3.2.3 Device band gaps

Since transmission and absorption measurements cannot be taken for a device, it is impossible to directly measure the band gap of the device with the same accuracy that films are. However, the normalized sub gap QE plot of two different samples can be compared to estimate the actual band gap if one of the devices has a known band gap. By comparing all devices to a known a-Si:H sample with a band gap of about 1.75eV, a good approximation of E04 gap and Taucs gap can be determined. In order for the measurement to be successful, the device must have an Urbach energy lower than 50meV and all device parameters such as thickness and normalized QE must have been taken. By shifting the plot so that the sub gap QE plots match, the shift will reveal the band gap of the material.

CHAPTER 4. RESULTS AND DISCUSSION

4.1 Semiconductor band gap

Optical band gap measurements for Taucs gap and E04 gap were measured on both devices and films. However, since the measurement for optical gap for devices is derived from a fitting routine that is governed by a reference film and device, these measurements should inevitably be consistent with films and will therefore be reported together. Standard devices with hydrogen dilution exhibit about 1.75eV for Taucs gap and 1.9eV for E04 gap. Films typically exhibited mid to upper 1.6eV Taucs gaps. However band gaps as low as 1.62eV were reported. Devices initially exhibited band gaps in the upper 1.6eV range, but later decreased when using TMB grading. The plot in Figure 4.1 shows the relative distributions of optical gaps for both devices and films during the progression of the research. As the deposition procedure was refined optical gaps began to decrease. Optical gaps varied by roughly for both films and devices. Initial films and devices yielded higher optical gaps, while later structures possessed lower optical gaps. Using optimized growth parameters, optical gaps can consistently be achieved with gaps lower than 1.64eV. Statistical information regarding Taucs optical gap can be found in Table 4.1.

Table 4.1 Population tauc gap statistics (eV)

Structure	**Mean**	**Minimum**	**25%**	**Median**	**75%**	**Maximum**
Devices	1.648	1.62	1.63	1.6525	1.6658	1.68
Films	1.663	1.63	1.6475	1.66	1.675	1.7

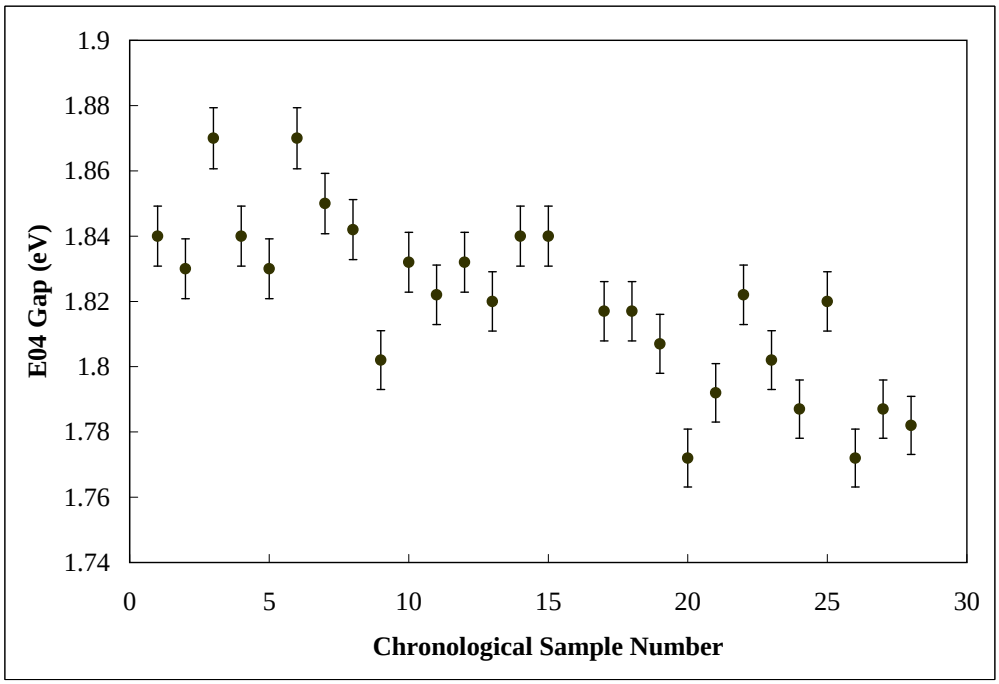

Figure 4.1 E04 gap distribution for devices and films versus chronological order of samples.

4.2 Film results

4.2.1 Growth rate

Growth rates of the intrinsic films grown under helium dilution and hydrogen dilution are shown in Figure 4.2. These results indicate that helium is marginally faster than hydrogen dilution, especially at higher pressures. This is a positive result for helium dilution because fast growth rates while maintaining high quality is desired.

4.2.2 Conductivity

Films grown initially had very meager photo/dark conductivity ratios. It was observed that these films exhibited very large photo current and very high dark current. This result indicated that some doping was occurring. It was hypothesized that oxygen may have been contaminating the films during the deposition so ppm TMB was admitted for later films. Films that were grown with admission of TriMethylBorate exhibited significantly better photo/dark

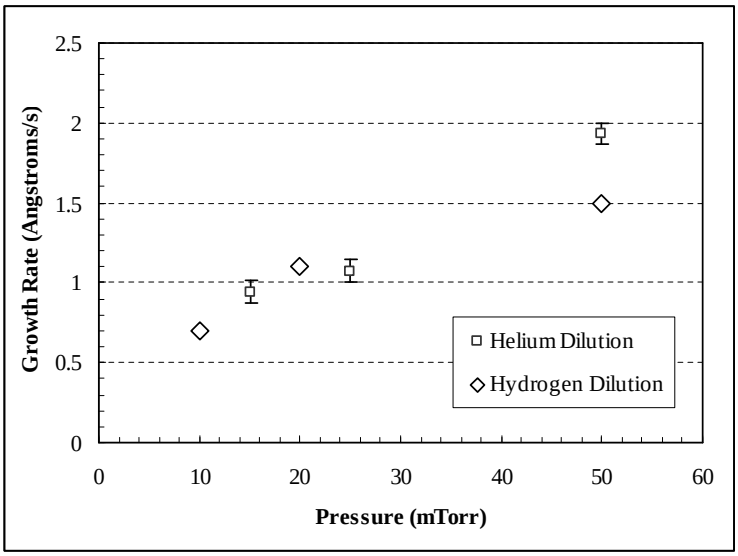

Figure 4.2 Growth rates with helium dilution versus pressure. Error bars denote 90% confidence interval.

conductivity ratios, but had lower light and dark currents. As expected, the ratio of photo and dark current ratios follow an exponential trend with activation energy, shown in figure 4.3. The improvement of photo and dark conductivity can be seen in table 4.2. This is an important result that indicates that during depositions for devices, admission of TMB may improve device quality, especially if used to grade the intrinsic layer doping.

Table 4.2 Film conductivity with TMB effects.

Sample	Photo current	Dark current	P/D ratio	Thickness	TMB
2-10922	$18.4\mu A$	$1.61nA$	1.14×10^4	$1.02\mu m$	No
2-11073	$17.0\mu A$	$.147nA$	1.16×10^5	$1.04\mu m$	No
2-11154	$1.66\mu A$	$2.73pA$	6.08×10^5	$.94\mu m$	Yes
2-11158	$.449\mu A$	$1.29nA$	3.48×10^5	$.94\mu m$	Yes

4.2.3 Hydrogen and oxygen content

FTIR indicated the expected result of lower hydrogen content in the amorphous structure. These results helped prove the low hydrogen content of the films grown that was originally sought after and expected. Figure 3.6 shows the resulting IR spectra for one of the helium

diluted films.

Hydrogen content for three films is displayed in Table 4.3. An assumed error of about ±1% is observed on hydrogen content measurements. The results indicate a very low hydrogen content of around 8% as expected. Films using hydrogen as a dilutant gas typically have hydrogen content greater than 10% if no chemical annealing techniques are performed. This low hydrogen content will have important positive implications on the band gap of the material. It should be restated that the errors in hydrogen content may be quite significant, as large as a percent in either direction due to unstable substrate temperatures and inconsistencies in the fitting routines. No clear temperature correlation was observed for hydrogen content over the range of 300°C to 400°C.

Table 4.3 also contains information about the ratio of SiH bonds to SiH_2 bonds. This is an important parameter to measure since it is desired to minimize the number of SiH_2 bonds. The results indicate that the ratio of SiH:SiH_2 is quite large. This is a desired result since the presence of SiH_2 bonds can manifest itself in the form of device instability[23].

Table 4.3 Hydrogen content and a-Si:H bond composition

Sample	**Temperature (°C)**	**H content**	**SiH:SiH_2 ratio**	**Substrate backing**
2-11136	300	9.25%	5.23	Aluminum foil
2-11147	375	7.71%	5.61	Stainless steel slide
2-11167	390	9.28%	4.89	7059 glass slide

FTIR data can also provide information about the presence of bonds with oxygen. Oxygen can be observed by the presence of a peak between 1000/cm and 1200/cm. Since this peak is very small on all FTIR results, it was not possible to quantify and reasonable measurement of oxygen content through bonding structure. Therefore the only deduction that can be made is that there is a negligible amount of oxygen present in the film. This is also an expected result because TMB was admitted during the deposition of all three films and TMBs reaction with oxygen is primary to incorporation in the film.

4.2.4 Activation energy

Activation energies of films grown with helium dilution differed significantly when using TMB during the deposition. Average activation energies can be seen in the Table 4.4. Activation energies of films grown with admission of TMB are about .8eV, which as expected is close to half of the band gap. Films grown without TMB typically possessed lower activation energies. This indicates that the films are likely doped n-type, possibly from oxygen contamination. The improved activation energy also improved photo/dark conductivity ratio Figure 4.3.

Table 4.4 Average activation energies

Film Description	Activation energy (avg.)
a-Si:H with TMB	.668eV
a-Si:H w/out TMB	.793eV

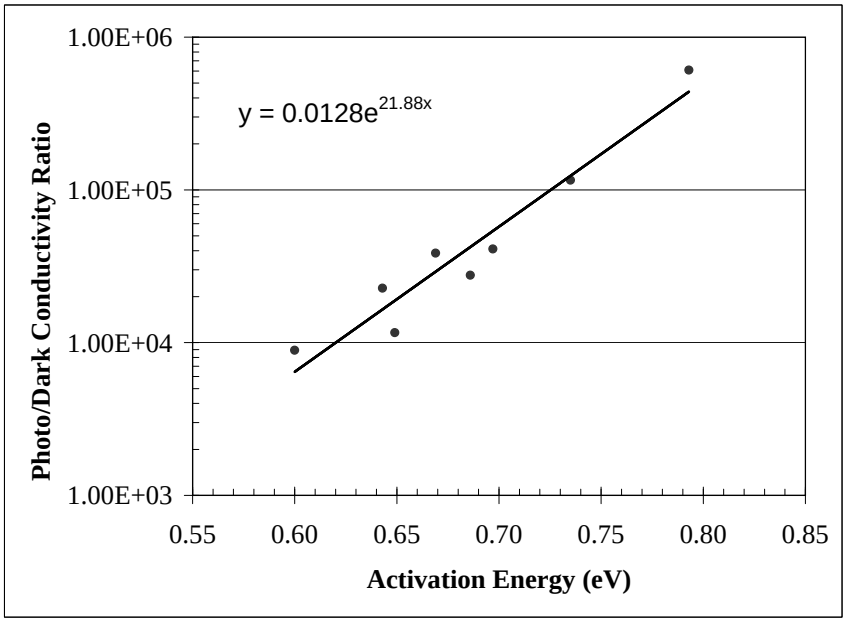

Figure 4.3 Photo/Dark conductivity ratios plotted versus activation energy.

4.2.5 Urbach energy

Film Urbach energy was typically larger for films, in the lower 50meV range. However, some films did exhibit mid 40meV Urbach energies. Figure 4.4 shows the film Urbach energies plotted against E04 gap. Figure 4.4 also shows that when obtaining lower band gaps, there is no clear sacrifice on material quality in the form of large Urbach energy.

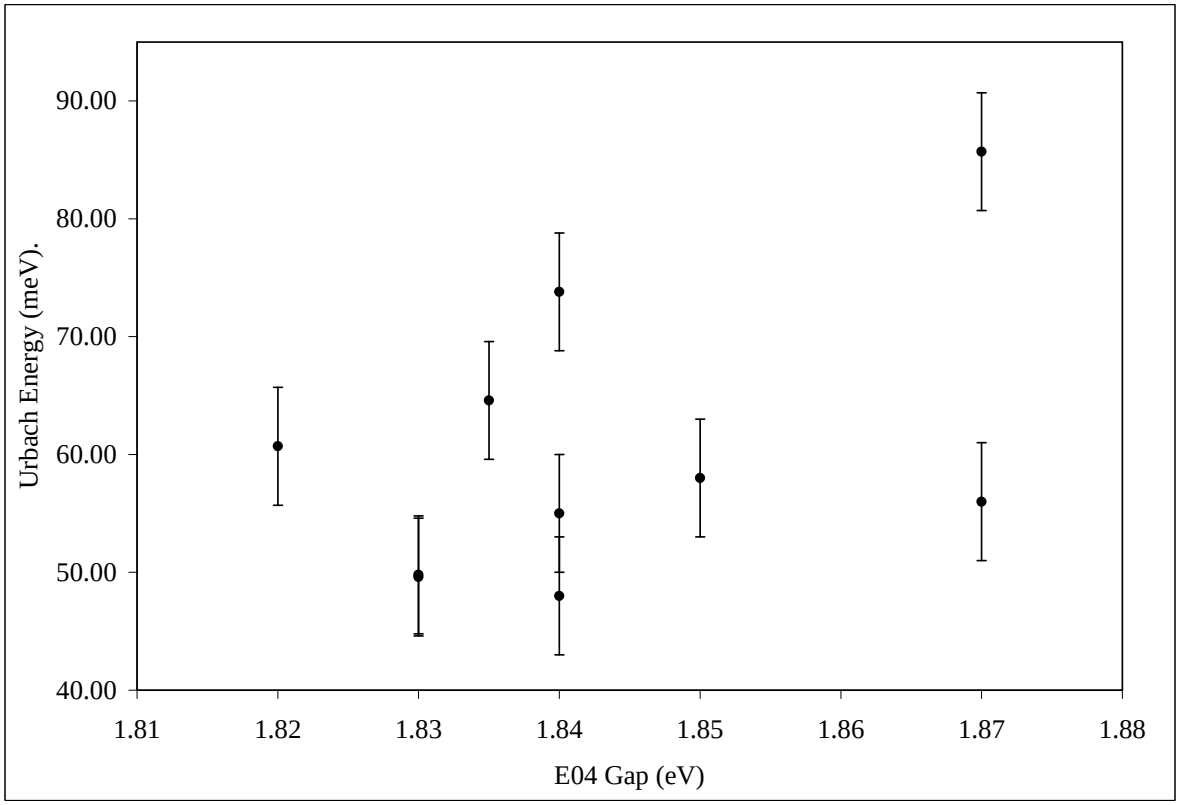

Figure 4.4 Urbach energy plotted versus E04 gap. Shows no clear trend between Urbach energy and optical gap.

4.3 Device Results

4.3.1 I-V curves and other electrical properties

Devices exhibited slightly lower V_{OC} than hydrogen diluted a-Si:H. This is likely due to the lowered hydrogen content of the intrinsic layer causing lowered optical gaps. Good quality devices exhibited reasonable current 1.3-1.4mA, however it was expected that this would be higher due to the lowered band gap. The lower than expected short circuit current I_{SC} is likely due to significantly higher defect density yielding a larger density of recombination centers. I_{SC} should increase if a method of decreasing defect density can be developed. Devices also exhibited low fill factors, typically between .52 and .56 (see Figure 4.6). As a reference, Figure 4.5 shows the IV curve of a good hydrogen diluted a-Si:H device. The reduced shunt resistance in Figure 4.6 is likely due to the lower $\mu\tau_{eff}$ product for holes, since they are not as easily collected under a smaller electric field.

An important trend that should be observed with band gap and V_{OC} is that it V_{OC} decreases with decreasing band gap (see Figure 4.6). This is because carriers that collect in the n+ and p+ region will alter the band structure so that diffusion currents can offset drift current more easily. That is, the potential of both the p+ and n+ regions do not have to change as much to approach the energy level of the conduction and valence band of the intrinsic material. On the other hand if a larger band gap existed in the intrinsic region, the n+ region potential would have to increase until it nearly matched the larger band gap materials conduction band. Therefore it would result in a larger open circuit voltage. This modest decrease in V_{OC} is expected to be offset by an increase in current due to a larger number of photo-generated carriers.

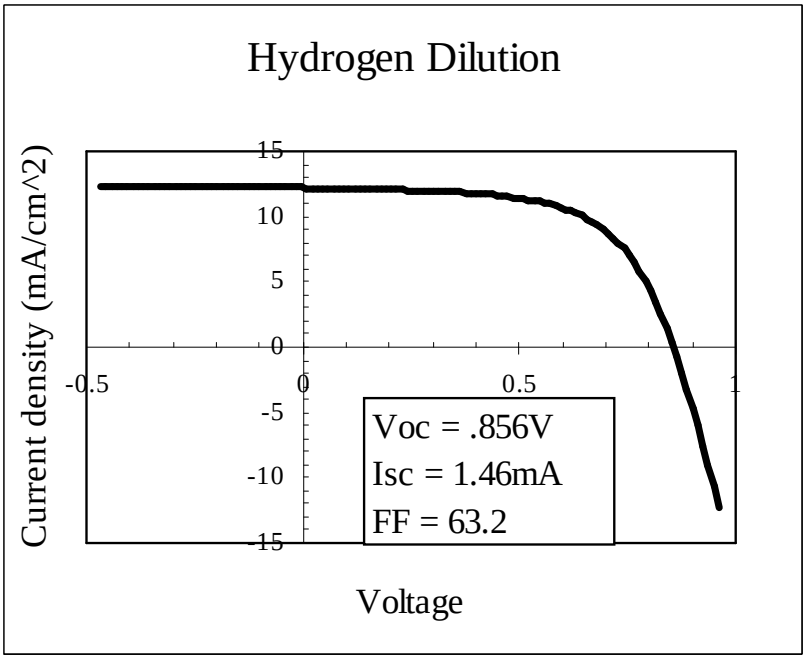

Figure 4.5 Hydrogen diluted sample IV curve.

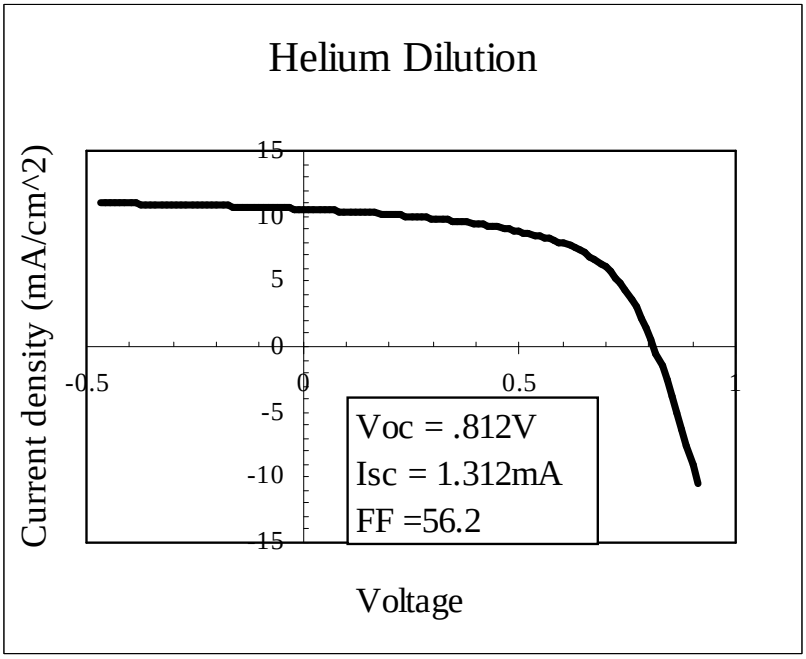

Figure 4.6 IV curve for helium diluted device possessing an optical gap of 1.63eV.

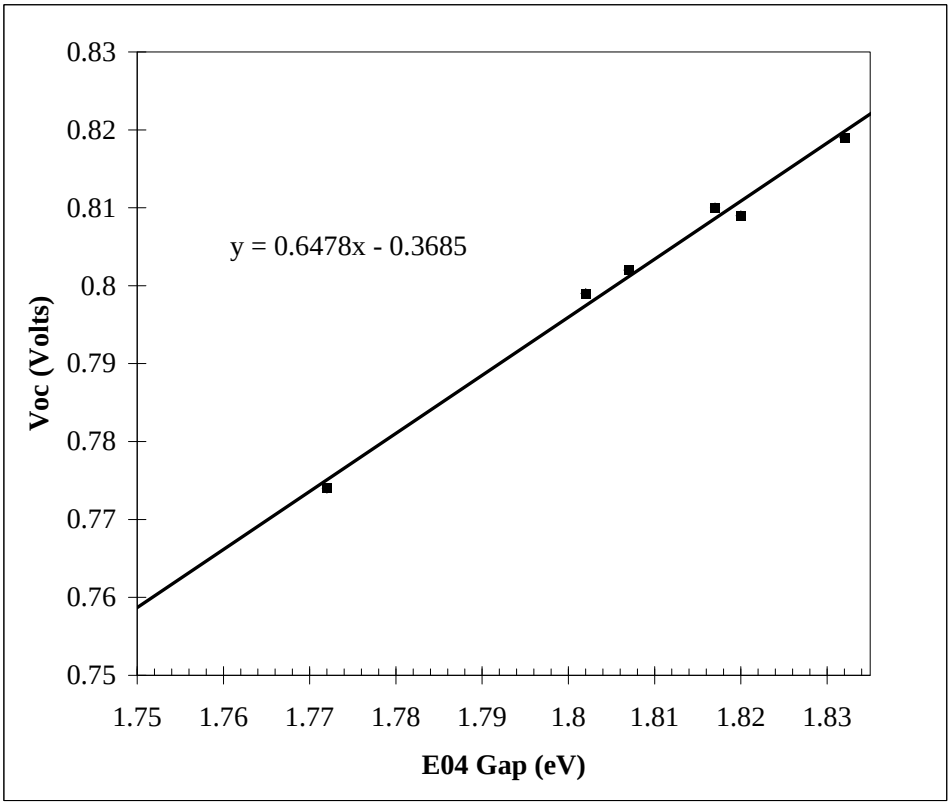

Figure 4.7 Voc plotted versus E04 Gap. Similar devices with varying optical gaps used for data.

4.3.2 Quantum efficiency

The results for QE indicate reasonable absorption at short wavelengths (>.4). At longer wavelengths, it is difficult to extract very much useful information about absorption; sub gap QE is used to provide that information. However the important parameter to look at is the ratio of QE when the cell is under zero bias and when it is under a bias of .5 volts. This shows how well the device will work when it is near its voltage of maximum power transfer.

The first QE plot (Figure 4.9) is of a device fabricated under helium dilution but without graded doping in i1 near the i1-i2 interface (see Figure 1.1 for relative location). Since the initial devices were fabricated without graded doping with TMB, collection of carriers at longer light wavelengths became a problem when the cell was under positive bias. This can be seen by the relatively high QE ratio at longer wavelengths. By using graded doping, collection can be enhanced at longer wavelengths yielding a more consistent QE ratio. This can be observed in Figure 4.10 where the device has graded doping near the i1-i2 interface. In the event that series resistance begins to increase for a cell, the short wavelength QE ratio generally increases significantly. The device in Figure 4.9 appears to have a minor series resistance problem which is likely near the i2-p+ interface. All devices fabricated under helium dilution including the two shown yielded peak absorption at 540nm. That means that these devices work best under conditions where visible light has the highest intensity. No correlation between optical gap and QE can be easily observed with this measurement technique.

By comparing the relative QE of helium dilution samples to hydrogen dilution samples, it becomes evident that there is clearly some hole collection problems ocurring. Figure 4.7 shows a hydrogen dilution device that possesses superior quality to the helium dilution samples. Both the helium and hydrogen diluted samples exhibited similar series resistances, therefore the large QE ratio shown in the plot of Figure 4.9 is likely due to insufficient collection of holes. This is a result of a poor $\mu\tau_{eff}$ product for holes.

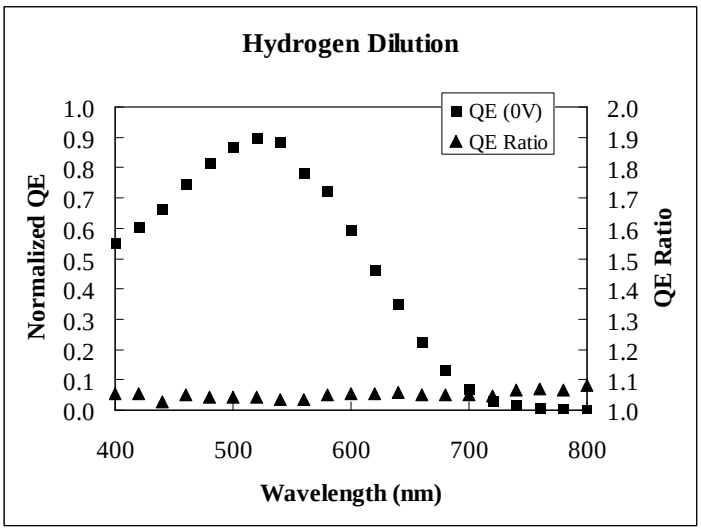

Figure 4.8 Hydrogen diluted sample. Normalized QE and QE ratio versus wavelength plotted. Device fabricated without graded doping.

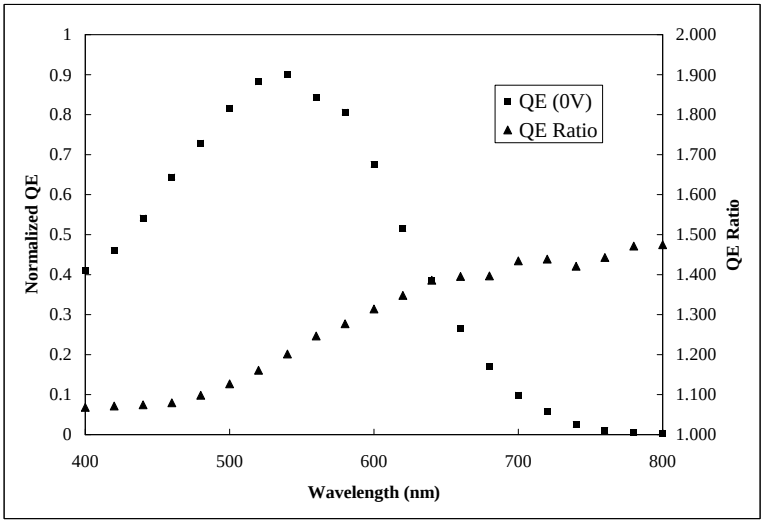

Figure 4.9 Normalized QE and QE ratio versus wavelength plotted. Device fabricated without graded doping. Device possesses an optical gap of 1.68eV.

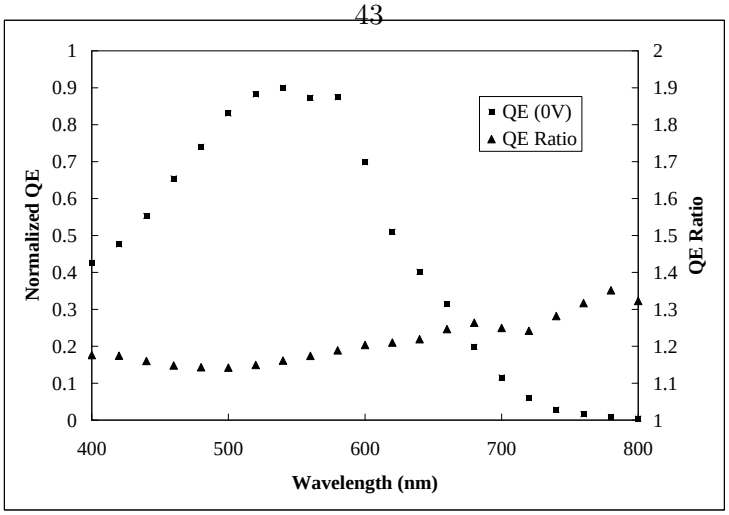

Figure 4.10 Normalized QE and QE ratio versus wavelength plotted. Device fabricated with graded doping in i1 near i1-i2 interface. Device possesses an optical gap of 1.63eV

4.3.3 Device sub gap QE and Urbach energy

Device Urbach energy yields nearly the same information that film Urbach energy does. For devices, it is much easier to approximate the linear region shown in Figure 4.11. Notice that there is a shoulder that appears between 1.3 and 1.4eV in Figure 4.11. This indicates the presence of mid gap trap states. These traps ultimately degrade the device. This shoulder was persistent through nearly all sub gap QE plots, indicating the presence of defects.

For devices, it was found that Urbach energies were significantly lower (Figure 4.12). This means that devices with sufficient material quality can be grown using helium dilution at 15mT. When plotted against E04 optical gap, there is no clear trend that can be drawn. However, this does serve to show that devices with low band gaps still possess usable characteristics. Futako [6] indicated that using argon ion bombardment, lower band gaps could be obtained. However, no comment was made about the quality of the devices and films produced under those conditions. This is an important result because it indicates that ion bombardment can produce low band gap devices without sacrificing material quality.

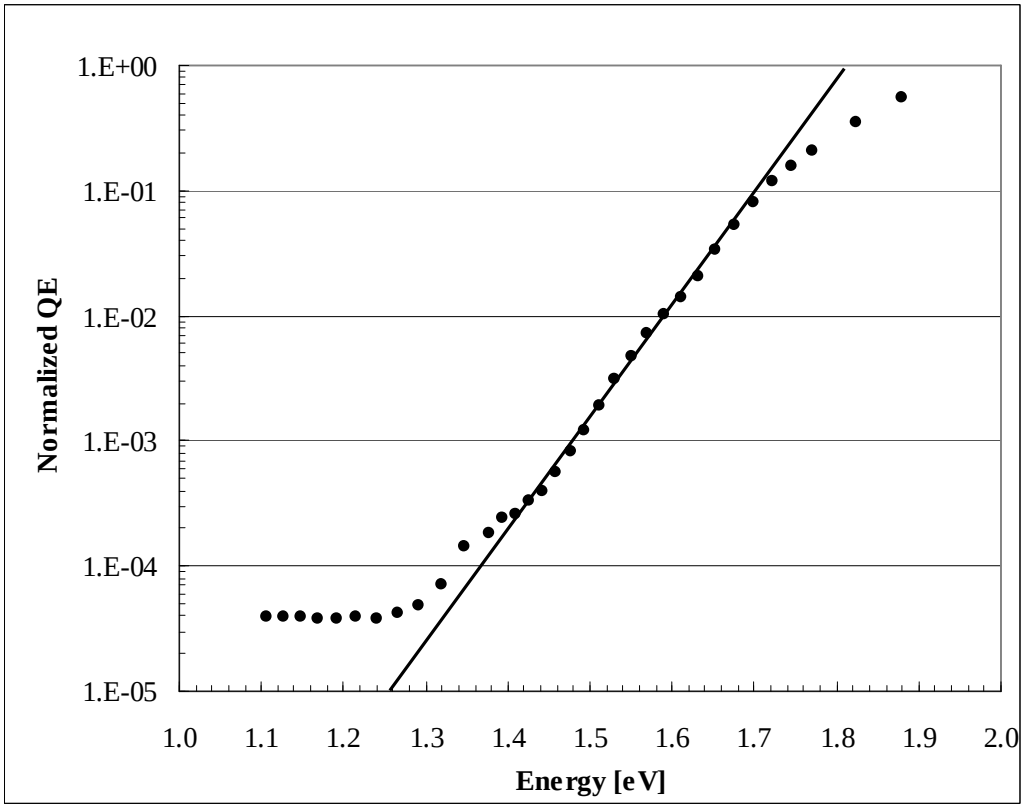

Figure 4.11 Sub gap QE plot showing Urbach energy linear extrapolation. Also indicating defects between 1.3 and 1.4eV.

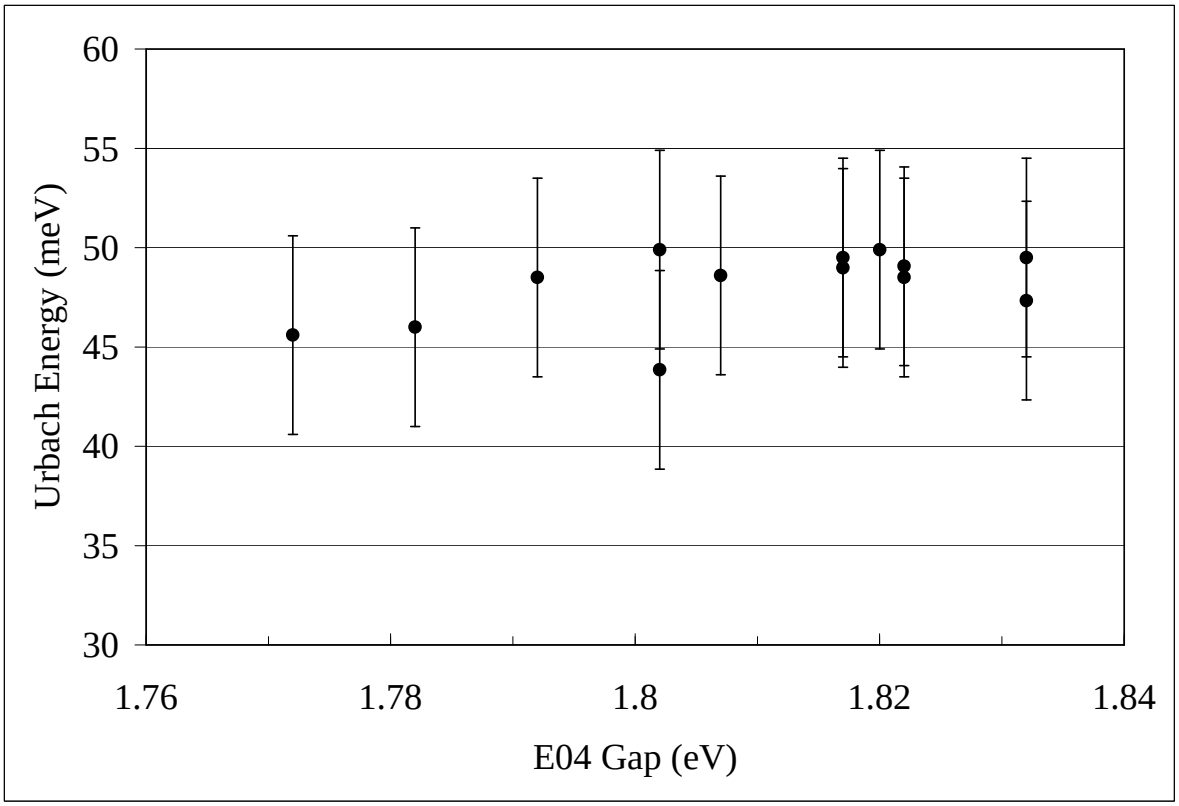

Figure 4.12 Device Urbach energy versus E04 gap.

4.3.4 Electron and hole $\mu\tau_{eff}$ products

The relative ability for a hole or electron to move through the intrinsic layer and not recombine can be expressed by the electron and hole $\mu\tau_{eff}$ products. This is measured for electrons by evaluating the expression:

$$\mu\tau_{eff} = \frac{\Delta\rho}{qG_{opt}} \tag{4.1}$$

Using films, electron mobilities are shown in Figure 4.13. Some electron $\mu\tau_{eff}$ products are within the expected range however the variation in $\mu\tau_{eff}$ product yields little conclusive information. Whether electron $\mu\tau_{eff}$ product is affected by varying levels of ion bombardment cannot be determined.

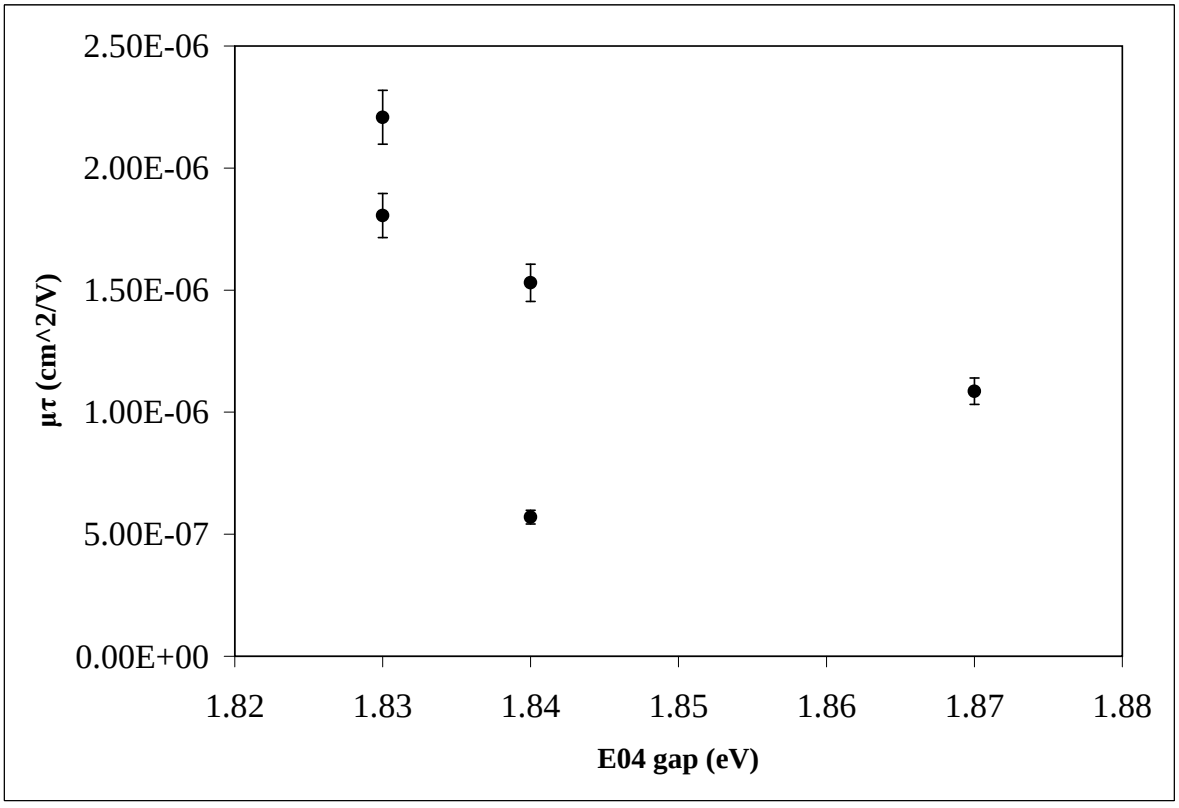

Figure 4.13 Electron $\mu\tau_{eff}$ versus E04 gap.

Hole $\mu\tau_{eff}$ product measurement is a bit more cumbersome. To measure hole $\mu\tau_{eff}$ products, a fitting of QE at varying voltages and wavelengths helps yield the hole $\mu\tau_{eff}$ product. Since hole $\mu\tau_{eff}$ product is considerably less than electron $\mu\tau_{eff}$ product (by at least 2 orders of magnitude) the only noticeable collection reducing mechanism for QE is the collection of holes. The expression for QE is the following:

$$QE(\lambda) = \frac{\alpha \cdot S_n}{1 + \alpha \cdot S_n}\left[1 - \exp\left(\frac{-t}{S_n}(1 - \alpha \cdot S_n)\right)\right] \tag{4.2}$$

Where:

$$S_n = \mu\tau E \tag{4.3}$$

With all variables known except for $\mu\tau_{eff}$, the product can easily be determined. Since this is a transcendental equation the simplest way to solve for $\mu\tau_{eff}$ is to use a fitting approximation technique. For devices, this yielded lowered hole $\mu\tau_{eff}$ products which were generally in the $10^{-9} cm^2/V$ range. Figure 4.14 shows the relationship of $\mu\tau_{eff}$ products for holes as bandgap changes. Notice that when using TMB graded doping near the i1-i2 layer, improvement in $\mu\tau_{eff}$ is observed.

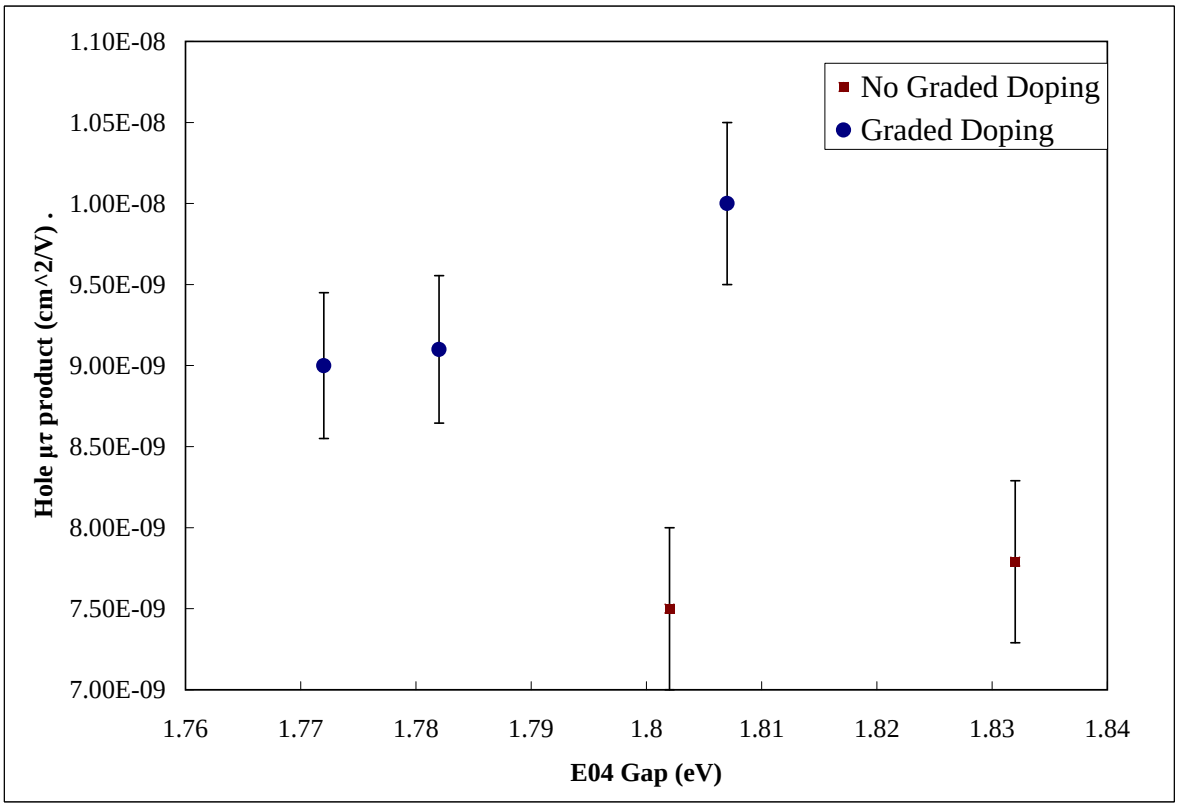

Figure 4.14 Hole $\mu\tau_{eff}$ products versus E04 gap with and without TMB graded doping in i2 near i1.

CHAPTER 5. CONCLUSIONS AND FUTURE WORK

PV cell fabrication with helium dilution at low pressures through this research has indicated some very promising results. Optical band gaps were consistently and easily brought to the low 1.6eV range without the use of germanium. This was confirmed by the low hydrogen content of films grown using the technique. The initial hypothesis that a reduction in hydrogen content could be realized by helium ion bombardment and that this would result in decreased optical gap was successfully verified. However, devices created exhibited poor quality compared to those of hydrogen diluted a-Si:H devices. The dimished performance was attributed to a lowered $\mu\tau_{eff}$ product for holes which resulted in poor carrier collection under bias. Further optimization should be able to consistently produce fill factors above 60 for helium dilution devices. Although devices possessed inferior performance, Urbach energies suggested that varying ion bombardment did not play a large role in producing inconsistencies in the amorphous structure. All devices and films exhibited reasonable growth rates keeping this technique cost effective. Since helium is frequently part of PECVD systems, no reactor modifications are necessary to use the technique.

There is still a sizable amount of work that is left to be done. The primary focus of any future work should be concerned with the reduction of the defect density of films grown under high ion bombardment conditions. This requires a more precise control of the level of ion bombardment. The data has indicated that it is likely that over-bombardment is the cause of the poor device properties. A different reactor design that uses a triode electrode arrangement could be used to control the level of ion bombardment. Also, further band gap reduction can be realized by using a chemical annealing technique for further bombardment.

This would come at the cost of lower deposition rate. Information about the stability of devices fabricated under these conditions and their susceptibility to the Staebler-Wronski effect should also be performed. Additional measurements should be performed to help steer subsequent experiments with this technique to yield low defect density devices with low band gaps. This would yield devices that would perform very well in tandem with other structures with textured substrates and back reflectors. This research is an initial step in providing a narrow band gap alternative to germanium alloyed devices.

BIBLIOGRAPHY

[1] A. Catalano, "Solar Cells made of Amorphous and Microcrystalline Semiconductors," Amorphous and Microcrystalline Semiconductor Devices, Ed. J. Kanicki, Norwood, MA: Artech House, Inc., 1991, pp. 9-76.

[2] A. Sherman, Chemical Vapor Deposition for Microelectronics, Park Ridge, NJ: Noyes Publications, 1987.

[3] H. O. Pierson, Handbook of chemical vapor deposition, Park Ridge, NJ: Noyes Publications, 1992.

[4] V. L. Dalal, "Fundamental considerations regarding the growth of amorphous and microcrystalline silicon and alloy films," Thin Solid Films, vol. 395, no. 1-2, pp. 173177, 2001.

[5] W. Futako, K. Yoshino, C. M. Fortmann, I. Shimizu, "Wide band gap amorphous silicon thin films prepared by chemical annealing," Journal of Applied Physics, vol. 85, no. 2, 1999.

[6] W. Futako, T. Kamiy, C. M. Fortmann, I. Shimizu, "The structure of 1.5 - 2.0 eV band gap amorphous silicon films prepared by chemical annealing," Journal of Non-Crystalline Solids, vol. 266-269, no. 1, pp. 630-634, 2000.

[7] W.E. Pickett, D.A. Papaconstantopoulus, E.N. Economou, "Theoretical study of optical absorption in hydrogenated amorphous silicon," Physical Review B (USA), vol. 31, no. 4, pp. 2232-2234, 1983.

[8] A. D. Zdetsis, E. N. Economou, D. A. Papaconstantopoulus, N. Flytzanis, "Electronic and transport properties of hydrogenated amorphous silicon," Physical Review B (USA), vol. 31, no. 4, pp. 2410-2415, 1985.

[9] T. Hama, H. Okamoto, Y. Hamakawa, T. Matsubara, "Hydrogen Content Dependence Of The Optical Energy Gap In a-Si: H," Journal of Non-Crystalline Solids (Netherlands), vol. 59/60, pp. 333, 1983.

[10] F. Zhu, J. Singh, "Approach to study the relation between optical energy gap and hydrogen concentration in hydrogenated amorphous silicon thin film," Journal of Applied Physics (USA), vol. 73, no. 9, pp.4709, 1993.

[11] N.F. Mott, E.A. Davis, Electronic Processes in Non-Crystalline Materials, Clarendon, Oxford, pp. 289, 1979.

[12] V.L. Dalal, J. Graves, J. Leib, "Influence of pressure and ion bombardment on the growth and properties of nanocrystalline silicon materials," Applied Physics Letters, vol. 85, no. 8, pp. 1413, 2004.

[13] A. R. Middya, S. Hazra, S Ray, "Growth of device quality amorphous SiGe:H alloys with high deposition rate under helium dilution," Journal of Applied Physics, vol. 76, no. 11, pp. 7578 1994.

[14] D.L. Staebler and C.R. Wronski, "Reversible conductivity changes in discharge-

produced amorphous Si," Applied Physics Letters, vol. 31, no. 4, pp. 292, 1977.

[15] A. V. Vasenkov, "Monte Carlo simulation of electron beam plasma in a silane-argon mixture," Journal of Physics D: Applied Physics, vol. 32, pp. 240-245, 1999.

[16] T. Pochett, A. Ilie, F. Foulon, B. Equer, "Charaterization of new a-Si:H Detectors fabricated from Amorphous Silicon deposited at high rate by Helium enhanced PECVD," Nuclear Science, IEEE Transactions on, vol. 41, no. 4, pp. 1014-1018, 1994.

[17] P. Roca, i Cabarrocas, J. B. Chvrier, J. Huc, A. Lloret, J. Y. Parey, and J. P. M. Schmitt, "A fully automated hotwall multiplasma-monochamber reactor for thin film deposition," Journal of Vacuum Science & Technology A, vol. 9, no. 4, pp. 2331-2341, 1991.

[18] S. Kaushal, V. L. Dalal, J. Xu, "Growth of high quality a-(Si, Ge): H films using low pressure remote ECR discharge," Journal of Non-Crystalline Solids, pp.198-200, 1996.

[19] Jianhua Zhu, Vikram L. Dalal, M. A. Ring, James J. Gutierrez and J. David Cohen, "Growth and properties of amorphous Ge:H solar cells," Journal of Non-Crystalline Solids, vol. 338-340, pp. 651-654, 2004.

[20] G. Myburg, R. Swanepoel, "The influence of substrate temperature on the deposition rate and optical properties of a-Si:H thin films prepared by rf-glow discharge," Journal of non-crystalline solids (Netherlands), vol.89, pp.341, 1987.

[21] Y. Hishikawa, S. Tsuda, K. Wakisaka, Y. Kuwano, "Principles for controlling the optical and electrical properties of hydrogenated amorphous silicon deposited from a silane plasma," Journal of Applied Physics (USA), vol. 73, no. 9, pp. 4227, 1993.

[22] Nanlin Wang "Improving the stability of amorphous silicon solar cells by chemical annealing," (PhD dissertation, Iowa State University, 2006)

[23] M.K. van Veen and R. E. I. Schropp, "Beneficial effect of a low deposition temperature of hot-wire deposited intrinsic amorphous silicon for solar cells," Journal or Applied Physics, vol. 93, no. 1, pp. 121, 2003.

[24] F. J. Kampas "Chemical Reactions in Plasma Deposition," Semiconductors and Semimetals, vol. 21, pp. 153-222, 1984.

[25] X. Deng and E. A. Schiff "Amorphous Silicon-based Solar Cells," Handbook of Photovoltaic Science and Engineering, Ed. A. Luque and S. Hegedus, John Wiley and Sons, Ltd, 2005.

[26] R. Swanepoel, "Optical functions of amorphous silicon," Properties of amorphous silicon and its alloys, Institution of Engineering and Technology, Ed. T. Searle, pp. 386-404, 1998.

[27] B.P. Nelson, H.M. Branz, R.S. Crandall, E. Iwaniczko, A.H. Mahan, P. Stradins, Q. Wang, and Y. Xu, (2003, May). "Project Summary of the NREL Amorphous Silicon Team," National Renewable Energy Laboratory, Presented at the National Center for Photovoltaics and Solar Program Review Meeting. [Online Document] ,[Cited 2008 March 14], Available HTTP: http://www.nrel.gov/docs/fy03osti/33564.pdf

[28] S. Guha, J. Yang, A. Banerjee, B. Yan and K. Lord, "High quality amorphous silicon materials and cells grown with hydrogen dilution," Solar Energy Materials & Solar Cells, 78 2003 pp. 329-347

[29] "United Solar Ovonic Technical Report," Uni-Solar, (2006, Oct.) [Online Document], [Cited 2008, March 14], Available HTTP: http://www.uni-solar.com/uploadedFiles/AA53606-02Technical%20Report120706small.pdf

[30] M. H. Brodsky, M. Cordona, J. J. Cuomo, "Infrared and Raman spectra of the silicon-hydrogen bonds in amorphous silicon prepared by glow discharge and sputtering," Physical Review B, vol. 16, no. 8, pp. 3556-3571, 1977.

ACKNOWLEDGEMENTS

There are so many people that I am compelled to thank for their companionship and contributions during this work. I would first like to thank my major professor Dr. Vikram Dalal for instilling passion, dedication, knowledge, persistence and encouragment toward my work. He also supported my work by funding this research. I would also like to thank Li Zhao and Max Noack for their training, support and patience. I would also like to thank Gary Tuttle and Mani Mina for serving on my committee and for inspiring me to pursue this work through their undergraduate courses. I also want to thank my fellow colleagues Michael Eggleston, Phil Reusswig, Bob Mayer, Atul Madhavan, Satya Saripalli, Dan Stieler, Ben Curtin and Ryan Boesch at the MRC for their friendship and frequent contributions to my work.

This work would not have been possible if it wasn't for the support of my mother and father Denise and Dennis Beckman. Their contribution to this work insurmountable because of their constant encouragment toward pursuing the things I enjoy. My sister Katie Beckman has been another companion that has always had the ability to motivate me and make me laugh and smile no matter what.